



# **Dynamic Amplification of Deformations in Railways due to High-Speed Traffic on Soft Ground**

**Søren Holm - Andreas Elkjær Riis**

**Master Thesis  
Master of Science in Structural and Civil Engineering  
Department of Civil Engineering, Aalborg University 2014**



**School of Engineering and Science**  
**Department of Civil Engineering**  
**Aalborg University**  
www.ses.aau.dk

Theme:  
Master's Thesis

Title:  
Dynamic amplification of deformations in railways due  
to high-speed traffic on soft ground

Project period:  
01-09-2013 to 10-06-2014

Supervisor:  
Lars Vabbersgaard Andersen, Aalborg University

Master students:



---

Søren Holm

---

Andreas Elkjær Riis

Copyright ©2014 are retained by the authors. All rights reserved. A copy can be downloaded for personal non-commercial research or study, without prior permission of the authors. This thesis cannot be reproduced or utilized in any format or medium, without obtaining prior permission of the copyright holders. When referring to this work, full bibliographic details including the authors, title, awarding institution and date of the thesis must be given.



# Prologue

This document includes the master's thesis made by Søren Holm and Andreas Elkjær Riis. The master's thesis is titled '*Dynamic amplification of deformations in railways due to high-speed traffic on soft ground*' and are presented in two articles.

In this document a review of the project is given, including a description of the problem considered and the main points from the two articles, which is also included in this document. The two articles are based on numerical simulations performed by the authors and the overall steps in the code forming the calculations are presented.

*Theory without practice is fantasy,  
practice without theory is chaos.*  
— Unknown

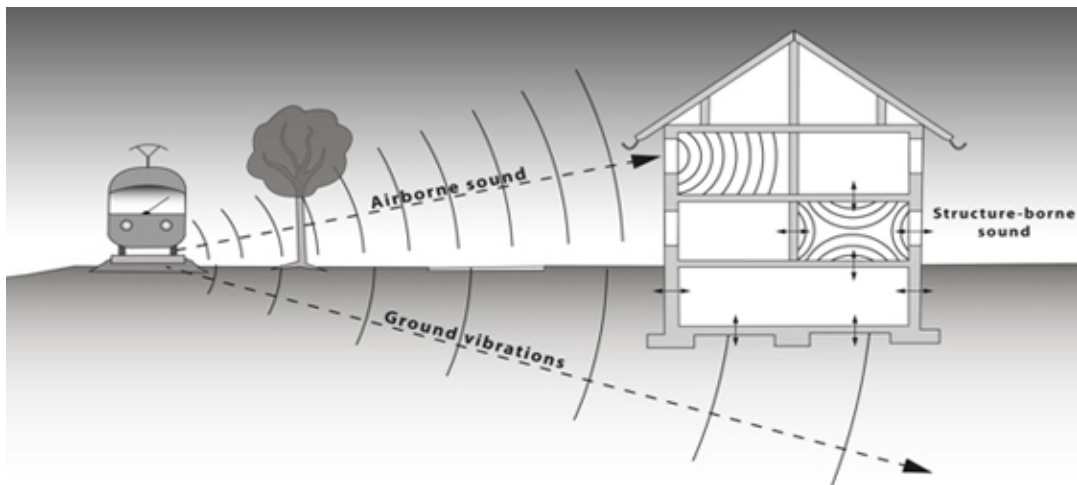


# Project Review



# Definition of project

Traditional geotechnics deals with static problems or slowly varying stresses in the soil, e.g. the consolidation theory. This project deals with geotechnics related to dynamics — geodynamics. Here focus is accelerations of the soil, which means that static equilibrium are not fulfilled. Acceleration of the soil may be caused by dynamic loads introducing wave propagation in the soil. Wave propagation in the soil can, for example introduced by earthquakes or traffic. Traffic induced vibration may be caused by the trains moving along a track on the ground surface. The vibrations generated by a moving train consist of airborne vibration, known as sound, and ground borne vibration. The ground borne vibration travels through the ground and may generate vibration in structures supported by the soil, and this may be felt by humans and can lead to damage on structures. Trains moving at high speeds may in special cases cause excessive vibrations, which raises concerns about the operation safety of the train, degradation of the embankment and the subsoil, and fatigue failure of the rails.



The background for this project is that an upgrade of the Danish railway lines is forthcoming. The lines should be upgraded in order to handle high-speed trains with a considerably higher speed compared to the trains operation today. Excessive vibrations may be induced if the operation speed of the train approaches the characteristic speeds for the wave propagation in the soil. The main topic in the project is related to the amplification of the vibration levels, a phenomenon which has been observed at several locations in other countries, due to an increase in the operation speed of the trains. Throughout this project, the amplification is denoted the *dynamic amplification* since it is introduced by means of dynamic effects.

Investigation of the dynamic amplification by an experimental approach is difficult and expensive. Thus, a numerical model may be preferable in order to clarify the phenomenon and investigate the influence of several parameters.

In this project a numerical model is developed and used for a parameter study. The configuration of the numerical model forms the background for the first part of the project. Numerical models can be very expensive in relation to computer power. Hence, in order to be able to perform calculations in a satisfactory amount of time, the simplicity of the model and the size of the model is an important consideration. The numerical model should be as simple as possible, but without ignoring the important features regarding wave propagation and the dynamic amplification. These challenges are treated in the first part of the project. Secondly, when a suitable numerical model is established, the inputs are very important in relation to obtain reliable results. This completes the first part of the project and forms the background for the second part of the project. The second part has focus on the importance of different input parameters. By this, the necessary effort to determine these parameters in a reasonable way is clarified. The effect of different input parameters are investigated through a parameter study.

# Summary

The substance of the project is presented in two articles. The first article deals with the development of a numerical model, which is able to simulate the ground response to a train moving upon an embankment along its surface. The second article deals with a parameter study, where the sensitivity of the ground response to different input parameters is investigated.

**Article #1** is titled '*Modelling of dynamic amplification of deformations in railways due to high-speed traffic on soft ground*'. In the first section an introduction to the phenomenon of dynamic amplification is given. A few locations where experimental measurements have been performed are mentioned and used to show the potential effects due of train speeds. The measurements performed at Ledsgaard are described in more details, due to the fact that the measurements are used as a validation tool for the numerical model. The second section is based on a litterature study of models used for similar simulations, where the concepts of modelling are outlined. Inspired by this, three different models are proposed in the third section, see Figure 0.1. The first model is widely used in situations of loads moving along a track. In the model, the track and embankment are represented by a Euler-Bernoulli beam and the soil is modelled as an elastic half-space. The two other models consider more advanced considerations regarding modelling of the track and embankment stucture. The two models are extended by application of Timoshenko beam elements, 2D continuum elements and continuous as well as discrete spring/damper systems. Numerical simulations performed using the three different models are presented in the fourth section. The simulations are compared to each other and to the measurements from Ledsgaard. In the fifth section, the conclusions regarding the numerical modelling and the simulations are outlined.

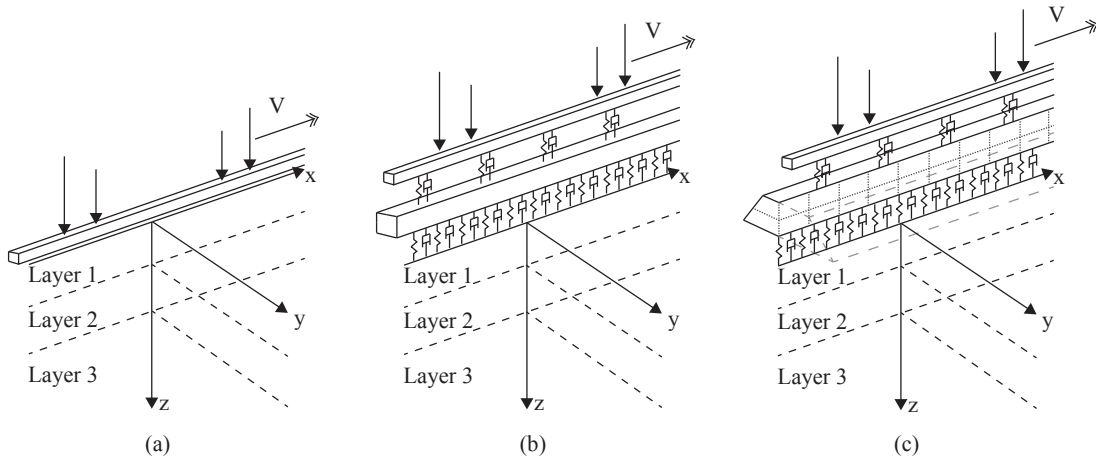


**Figure 0.1.** The track-embankment system on the soil in the numerical models.

**Article #2** is titled '*Parameter study of dynamic amplification of deformations in railways due to high-speed traffic on soft ground*'. In the first section, a general introduction is given. This includes a slightly more detailed description of some of the observations made from experiment as well as computational models regarding dynamic amplification. A brief introduction to some of the effects being important in relation to wave propagation in homogeneous and layered soil media are presented. Finally, the first section contains a short literature study regarding numerical models which are verified using the data from the Ledsgaard site.

The most simple model outlined in the first article is adopted in order to perform the parameter study. In the second section, the model is briefly described. In the third section some reference cases are set up. The reference cases are used as a basis for comparing the results from the parameter study, and they contain homogenous soil profiles as well as two-layered soil profiles. The soil profiles are based on materials of peat, clay and sand. The parameter study is performed in the fourth section. Some of the input parameters for the soil in the numerical model are varied as well as the influence of the stiffness of the embankment is investigated. For the situation of a two-layered soil profile, the thickness of the top layer is studied. Comparisons and comments to the results are also presented in this section. The main observations include the importance of the stiffness of the soil layers and the above structure and also the height of the top-layers, whereas other soil parameters are of minor importance in relation to the dynamic amplification. Finally, the conclusion of the parameter study is given in the fifth section.

## Conclusion

It is a challenging task to construct a numerical model that reproduces the measurement from Ledsgaard. However, constructing a model with the potential to reproduce the measurement is successfully achieved in this project. A number of assumptions are made in the numerical model, and the information regarding some of the input parameters in the model is inadequate. However, two of the three models succeeded reproducing the pattern of response in a satisfactory way, providing the belief that the amplitude of the displacement response can be reproduced more correctly by calibrating the model.

The first model is the most simple with the smallest number of inputs. The first and the second model produces the same results, whereas the third model does not reproduce the phenomenon of dynamic amplification in a satisfactory manner. Hence, the most advanced model is not necessarily the best model. It might have the potential to reproduce the measurements, but due to the fact that the number of input parameters are greater than in the simple model, the calibration would be a more challenging process.

During the parameter study it is found that the dynamic amplification is highly dependent on the soil stratification. A homogeneous soil profile is preferable compared to a layered soil profile with a soft soil in the top layer. Studying the influence of the soil parameters reveals that the stiffness of the material is an important parameter, whereas the damping ratio and Poisson's ratio are of minor importance regarding the dynamic amplification. However, the damping ratio influences the response considerably when the train has passed. A higher damping ratio, obviously, results in higher damping, i.e. the free oscillations produced by

the passing train are damped more quickly.

The final conclusion is that, in order to reproduce the measurements from the Ledsgaard site more accurately, a calibration process should be performed regarding the numerical models. Furthermore, in studies of the dynamic amplification the focus should be on determination of the stiffness of the soil and the soil stratification, as the parameter study reveals that this is the most important parameters regarding the behaviour of the soil.

## Program Review

The simulations performed during this project are made by use of a numerical code designed by the authors. The code is established in MATLAB using a FORTRAN execution. The steps in the numerical simulations are as follows:

1. The inputs to the model are defined.
2. The topology of the system is established.
3. The loads are established and the time series are converted from time domain to frequency domain by means of Fourier transformation.
4. From the topology of the system, the Green's function is calculated in the points of interaction between the track-embankment structure and the ground. It is calculated at the frequencies corresponding to the transformed load. This part of the calculations is conducted using FORTRAN.
5. The finite element matrices of the track-embankment elements are calculated and assembled into the global system.
6. Utilizing the formulation in frequency domain the system matrices are transformed to a dynamic stiffness and the stiffness of the soil, obtained by means of Green's function, are added to the dynamic stiffness of the system.
7. From the dynamic stiffness and the transformed load, the displacements in the frequency domain are calculated.
8. The response in time domain are obtained from the inverse Fourier transformation.

The numerical models have some limitations; the train has constant velocity, the dynamic of the train is not included since the train is modelled as a series of single loads decoupled from the track. The track-embankment structure is modelled as a straight and horizontal structure, and motions across the embankment are not included. The loads from the embankment to the soil are assumed as a Gaussian formed distribution in the longitudinal as well as the transverse direction. Regarding the soil, the model only accounts for horizontal layers and isotropic and homogeneous materials having a linear elastic behaviour.

Future steps in the improvement of the model might be a more realistic modelling of the train and the loads, where the interacting between the rails and the train is accounted for. Modelling the train as part of the model could also be used to estimate the vibration levels in the train. The load distribution from the embankment to the soil could form the basis of an exhaustive investigation. An interesting improvement would be the development of a 3D model, in order to assess the quality of the assumption made in the 2D formulation.



# Article I



# Modelling of dynamic amplification of deformations in railways due to high-speed traffic on soft ground

Søren Holm<sup>◦</sup> Andreas Elkjær Riis<sup>◦</sup>

Lars Vabbersgaard Andersen<sup>•</sup>

*Master students<sup>◦</sup> and associate professor<sup>•</sup> at  
Department of Civil Engineering, Aalborg University, Denmark*

---

## Abstract

Three numerical models to analyse ground vibrations due to high-speed trains are presented. In the numerical models, the rails, the embankment and the ground are considered. The ground is modelled as a half-space in all the models and the transfer-matrix method is applied to obtain the Green's functions. In the first model, the rail-embankment system is modelled using a Euler-Bernoulli beam. In the second model, the rails are modelled as a Euler-Bernoulli beam and the embankment is modelled as a Timoshenko beam, where spring/damper systems are applied as coupling between the different parts of the system. In the third model, the rails are modelled as a Euler-Bernoulli beam and the embankment is modelled as a continuum. The case at Ledsgaard in Sweden, where large increases in vibration level were observed due to an increase in train speed, are used for validation of the models. In the simulations performed, model three is a comparatively unaccurate model, whereas the two other models follow the same pattern as the measurements, however, overestimating the displacement amplitudes. The influence of modelling the train with either bogie loads or axle loads is investigated, and finally it is demonstrated that the dynamic effects are also generated in the case of a single load moving along the railway track.

---

## 1 Introduction

The first railway line in Denmark opened in 1847 and was serviced by a steam locomotive at a speed of 50 km/h. In 1860 a law on railway tracks was adopted and within 10 years, Denmark was covered with a network of railway tracks. These are roughly the tracks which represent the location of the railway lines today ([Jernbanen.dk](#)).

Due to the limited speed of the trains, the original location of the railway tracks did not consider the recently discovered effects of high-speed trains. Further, today's demands for higher train speeds to shorten travel times call for straight railway lines. Due to these circumstances, crossing of soft soil areas are unavoidable and soft-soil sites are particularly susceptible to excessive vibration from high-speed trains. Thus, an important consideration is to investigate the dynamic effect of a high-speed train because there is little experience of the phenomenon in Denmark.

Significant increase has been observed in the vertical movement of the track by railway companies throughout Europe for increasing train speeds. Unfortunately, the amount of data from performed measurements are hardly available in the literature.

However, Woldringh and New (1999) report on data from a few measurements. The data is from measurements at Stilton Fen in the United Kingdom, Amsterdam-Utrecht in the Netherlands and Ledsgaard in Sweden. From the measurements it is evident that the increase in vertical movement at high speed can be at least two or three times the vertical movement at low speeds.

### 1.1 The Ledsgaard site

At the Ledsgaard site in Sweden, high vibration levels were observed in 1997 in connection with maintenance work close to the track, and comprehensive investigations were performed in order to clarify the phenomenon and understand the mechanism of the behaviour. The investigations consisted of a test run programme regarding the train loads and a characterization programme with respect to the soil properties at the location.

The characterization programme was performed to establish the soil profile and the geodynamic parameters of the soil layers and the embankment. The embankment is 1.4 m thick and consists of 0.5 m crushed bedrock and 0.9 m gravel. The site can be characterized by a 1.5 m dry weathered crust layer

over a 3.0 m thick layer of soft organic clay. Under the soft organic clay, a deposit of soft marine clay is present, having a thickness of more than 50 m and beneath this bedrock is present (Adolfsson et al., 1999).

The test run programme was performed by the Swedish National Rail Administration (BANVERKET) using an X2000 passenger train consisting of an engine and four cars, having a total length of approximately 109 m. A total of 20 test runs was performed, including northward as well as southward runs. In each test run the speed of the train was constant and ranging from 10 to 204 km/h. Electronic displacement transducers were placed along the track, and accelerometers, seismometers and pore pressure sensors were located at various depths and distances from the track in order to measure the displacements, accelerations, velocities and pore pressure. Details on the instrumentation are reported in the work by Adolfsson et al. (1999).

## 1.2 Dynamic amplification due to moving loads

From an analysis of the recorded data, Madshus and Kaynia (2000) and Kaynia et al. (2000) decompose the displacement field into a quasi-static and a dynamic field, which is stationary relative to the train. The quasi-static field contains only downward motion and its pattern does not change with the train speed. The dynamic field contains both upward and downward motions, having equal displacement amplitude. It has a tail of free oscillation following the train, and the propagation speed of this field is identical to the train speed. For high-speed train passages, the dynamic field dominates the response, and the embankment and the ground behave non-linearly due to large strains.

According to Krylov (1995) the large increase in ground vibration is due to the effect of moving sources approaching the velocity of the Rayleigh surface waves propagating through the ground. In a soil medium both compression and shear waves propagate, having the following phase velocities, respectively:

$$c_P = \sqrt{\frac{\lambda + 2\mu}{\rho}} \quad , \quad c_S = \sqrt{\frac{\mu}{\rho}},$$

where  $\rho$  is the mass density and  $\lambda$  and  $\mu$  are the Lamé constants given by

$$\lambda = \frac{\nu E}{(1 + \nu)(1 - 2\nu)} \quad , \quad \mu = \frac{E}{2(1 + \nu)}.$$

Here  $E$  is Young's modulus and  $\nu$  is Poisson's ratio. Since the Lamé constants and the mass density are positive,  $c_P > c_S$ . For a moving load on a medium the apparent wave propagation velocity as observed from the source will be different in different

directions. This is the so called Dobbler effect (Ballard, 2010). The significance of the effect depends on the phase speed of the waves in the medium and the speed of the moving load. The speed of the moving load in relation to the phase speeds leads to three different cases: subsonic motion ( $v < c_s$ ), transonic motion ( $c_s < v < c_p$ ) and supersonic motion ( $c_p < v$ ). When an interface or a free surface is present, mixing of the two basic wave types takes place. Rayleigh waves is an example of this and is a wave front propagating along the surface of the medium. According to Andersen (2006) the Rayleigh wave speed is 0.862-0.955 times  $c_S$  depending on the Poisson ratio.

When a train moves on the surface of a homogeneous half-space at a speed equal to or higher, than the Rayleigh wave speed, a Mach cone forms behind the train. Further, as the train speed approaches the Rayleigh wave speed, large dynamic amplification of the displacement response occurs. However, for a train moving on a track and embankment over a homogeneous or layered ground, the problem appears to be more complicated. Based on the assumption, that the track-embankment system and the ground can be modelled as a beam interacting with a homogeneous half-space Dieterman and Metrikine (1996) found that there should be two critical speeds, one equal to the Rayleigh wave velocity of the ground, and the other, fairly close to the first, depending on the stiffness and mass of the track-embankment system and the ground properties. The report on data by Woldringh and New (1999) indicates that the dynamic effects are introduced when the train speed is around 60% of the critical speed at the location, and that the effects increase as the train speed is approaching the critical speed.

Soft sandy soils may have Rayleigh wave velocities as low as 320-470 km/h, (Krylov, 1995). For peat, organic clays, and soft clays it can be as low as 110-180 km/h, (Woldringh and New (1999) and Madshus and Kaynia (2000)). Due to the fact that the velocity of Rayleigh surface waves in soft soils can be considerably lower than the design speed of the railway lines nowadays, problems regarding train speeds approaching or even exceeding the critical speed can be expected to an increasing amount.

## 1.3 Paper summary

The aim of the paper is to make a numerical model which is capable of predicting ground vibrations due to a series of moving loads. In Section 2 concepts of modelling are presented and this forms the basis in the proposal of a numerical model. In Section 3 the governing system of equations are introduced and the solution procedure is outlined. The numerical model consist of a series of loads corresponding to a train, the track and embankment and finally the ground. The modelling of the train loads are

described in Section 3.1 while the modelling of the track-embankment system and the soil are presented in Section 3.2 and Section 3.3, respectively. In Section 3.2 three different proposals for a numerical model are presented. Field measurement from the Ledsgaard site in Sweden are used as a validation tool for the models. The results from the simulations are presented in Section 4 and the accordance between the simulations and the measurements are discussed.

## 2 Concepts of modelling

The comprehensive investigations at the Ledsgaard site has provided an excellent opportunity to validate numerical models simulating a series of loads moving along the ground surface. The dynamic interaction of train, track and soil is a complicated problem and generally several simplifying assumptions are made in numerical models. The modeling of the system is often performed using a beam on elastic foundation because of simplicity and availability of analytical solutions for loads moving at constant velocity. Winkler and Kelvin foundations are widely applied elastic foundations, e.g. by Andersen et al. (2001) and Paolucci et al. (2003), but the fact that they are unable to transfer the energy along the track makes them inadequate for modelling tracks resting on soils. Modelling the soil as an elastic layer or a half space, as done by e.g. Kaynia et al. (2000) and Takemiya (2003), seems as a more realistic approach.

Modelling the soil as an elastic layer can e.g. be achieved through the finite element method, cf. (Zienkiewicz et al., 2005), (Bathe, 2007) and (Cook et al., 2001), or the boundary element method, cf. (Dominguez, 1993) and (Beskos and Manolis, 1988). The finite element method may advantageously be applied in analyses of wave propagation in media with complex material behaviour and local inhomogeneities. However, by applying finite elements only a limited area/volume can be modelled, thus the radiation damping cannot be accurately accounted for. This can be mended by use of transmitting boundary conditions, e.g. (Zhenpeng, 2001), infinitesimal finite element cell method, e.g. (Wolf and Song, 1998) or semi-infinite elements, e.g. (Bettess, 1992). Alternatively, the boundary element method provides the capacity of accurately modelling the radiation damping, thus it may advantageously be applied for analysis of large open domains, e.g. (Galván and Domínguez, 2007) and (Andersen and Nielsen, 2003).

Due to, for example, transient loading or nonlinear material behaviour, the variation in time is an important consideration in the analysis. However, making the analysis in the time domain is expensive in terms of computation time. Fortunately,

in the case of linear response Fourier transformation provides an alternative, namely the frequency-domain solution, which concerns steady state response. The time-domain solution can be obtained from the frequency-domain solution by inverse Fourier transformation without loss of generality. In the frequency-domain solution a set of equations appear, which can be handled individually and analytically in a computationally efficient manner. Similarly, the spatial domain can be transformed utilizing the Fourier transformation given that the ground can be treated as a horizontally layered half-space. This way the partial differential equation of motion for the soil may be reduced to an ordinary differential equation in terms of the depth coordinate, making an analytical solution accessible. The transfer-matrix method, which has been widely applied in the analysis of loads moving on the surface of horizontally layered soil, utilizes this formulation (Thomson (1950), Haskell (1953) and Sheng et al. (1999)).

Several authors have used the data from Ledsgaard to validate their numerical models. Only authors using the domain transformation method followed by inverse Fourier transformation will be cited in this section. Kaynia et al. (2000) and Paolucci et al. (2003) modeled the track-embankment system and the ground as a beam interacting with a horizontally layered viscoelastic half-space and a beam interacting with an elastic foundation, respectively. For points located on the track, the simulations reproduce the measurements regarding pattern as well as amplitude. Madshus and Kaynia (2000) use the same model as Kaynia et al. (2000) except from using an equivalent linear approach to account for the materials to behave nonlinearly. The simulations agree largely with the measurement; particularly the pattern of the response has good agreement. Takemiya (2003) modelled the track-embankment system as a Euler-Bernoulli beam and the ground as a layered viscoelastic half-space also using an equivalent linear approach to account for the materials to behave nonlinearly. For train speeds well below the critical velocity the model predictions and the measurements fits very closely, but for train speeds approaching the critical velocity, the deviation increases highly. Karlström and Boström (2006) modelled the rails as Euler-Bernoulli beams and the sleepers are modelled with an anisotropic Kirchhoff plate. The ground is modelled as a stratified half-space with linearly viscoelastic layers and the embankment is also modelled as a viscoelastic material. The simulations reproduce the measurements, especially for low train speeds the simulations agree almost exactly with measurements. Costa et al. (2010) modelled the embankment and the ground by 2.5D finite elements. The 2.5D finite element method differs from the transfer-matrix method in the sense that Fourier transform is only applied with respect to time and

the spatial coordinate along the track. The resulting partial differential equation is solved by the finite element method. The rails are modelled by Euler-Bernoulli beams connected to the embankment by a spring/damper system, representing the rail pads. The simulations are performed with and without nonlinear effects taken into account by an equivalent linear approach. Very good agreement is obtained including the nonlinear effects, while the amplitudes are underestimated when excluding the nonlinear effects.

### 3 Numerical modelling

Based on the previous section, three different numerical models are investigated by the authors of the present paper. The aim is to simulate the situation illustrated in Figure 1 and compare and validate the models using the measurements from Ledsgaard. The numerical models consist of a finite element

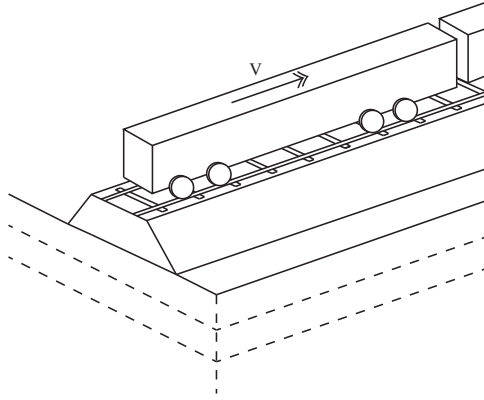


Figure 1: A part of the train moving along the railway system comprising the rails, embankment and the ground.

model of the track-embankment system interacting with an elastic half-space representing the soil. In all models, the soil is modelled using Green's function for the layered half-space, thus the difference between the models lies within the finite element modelling of the track-embankment system. In the first model, the track-embankment system is modelled as a Euler-Bernoulli beam. In the second model, the track is modelled as a Euler-Bernoulli beam, while the embankment is modelled as a Timoshenko beam. The reason for this is that Euler-Bernoulli beams apply for thin beams, and the depth of the embankment is significant, meaning that shear deformation should not be disregarded. In the third model the track is modelled as a Euler-Bernoulli beam and the embankment is modelled as continuum finite elements assuming plane stress over the width of the embankment. An illustration of the three models is given in Figure 2.

Due to utilization of the transfer-matrix method, the analysis is carried out in frequency domain. The

circular frequencies  $\omega$  considered in the frequency-domain are dictated by the discrete time series in the time domain. The solution is found to each frequency by the governing equation,

$$\tilde{\mathbf{K}}(\omega) \tilde{\mathbf{U}}(\omega) = \tilde{\mathbf{F}}(\omega) \quad (1)$$

where  $\tilde{\mathbf{U}}(\omega)$  and  $\tilde{\mathbf{F}}(\omega)$  are vectors of the corresponding Fourier transforms of the discrete time series for the displacement and load, respectively, and  $\tilde{\mathbf{K}}(\omega)$  is the corresponding dynamic stiffness matrix:

$$\tilde{\mathbf{K}}(\omega) = -\omega^2 \mathbf{M} + i\mathbf{C} + \mathbf{K} \quad (2)$$

Here  $\mathbf{K}$ ,  $\mathbf{M}$  and  $\mathbf{C}$  are the stiffness, mass and damping matrices of the system, respectively. These matrices are obtained directly from a finite element formulation of the system. However, the soil is modeled using Green's function instead of a finite element formulation, hence, only the dynamic stiffness related to the track-embankment system can be found using Equation (2). As described in Section 3.3 using Green's function gives a complex stiffness matrix,  $\tilde{\mathbf{H}}(\omega)$ , of the soil, which can be combined with the dynamic stiffness matrix from the finite element formulation. The governing equation to be solved is then given by (1) with

$$\tilde{\mathbf{K}}(\omega) = \begin{bmatrix} \tilde{\mathbf{K}}_{11}(\omega) & \tilde{\mathbf{K}}_{12}(\omega) \\ \tilde{\mathbf{K}}_{21}(\omega) & \tilde{\mathbf{K}}_{22}(\omega) + \tilde{\mathbf{H}}(\omega)^{-1} \end{bmatrix} \quad (3)$$

where  $\tilde{\mathbf{K}}_{22}$  refers to the three translational degrees of freedom in each node which combines the soil and the finite element formulation of the track-embankment system and  $\tilde{\mathbf{K}}_{11}$  refers to the remaining degrees of freedom in the system.

From the displacement vector in the frequency domain, the time series response is found by inverse Fourier transformation.

#### 3.1 Modelling of the train loads

The interaction forces between the train and the rails, in reality, consist of a quasi-static term and a dynamic term. The quasi-static term is constant due to the weight of the train. The dynamic term is varying in time due to track irregularities and vehicle defects, e.g. wheel flats. The actual interaction force is therefore extremely complex due to the dynamic term, thus, the train is decoupled from the track and the dynamic term is omitted in the present analysis which has focus on the effects of the train speed relative to wave propagation velocities in the track-embankment-subsoil system. The loads from the X2000 passenger train used for the test programme at Ledsgaard are modelled using a series of forces of constant magnitude moving with constant speed  $v$ . The axle spacing distances and loads corresponding to the X2000 passenger train is illustrated in Figure 3. The loads are illustrated

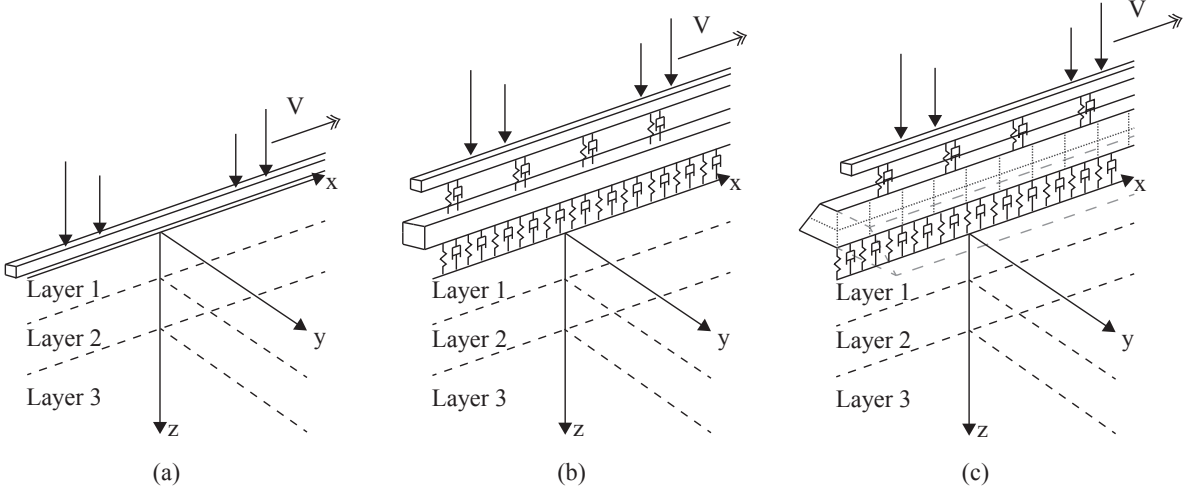


Figure 2: The track-embankment system in the numerical models.

as both axle loads and bogie loads, i.e. the bogie load is the sum of the two associated axle loads. The total length of the train is approximately 109 m. The length of the numerical model is partly dictated by the length of the train. The second part having influence is the length for the train to travel in the model before reaching a stationary condition, meaning that the effects due to initialization of the moving loads in the system are not present. The third part having influence is that the entire train should pass a section of the model and move far enough behind it in order to ensure that the section do not feel the loads from the train anymore.

The discrete time series in the numerical model depends on the speed of the train. In the present analyses, the time step is dictated by the condition that the train travels the distance between two nodes in the numerical model using four time steps. When the loads are present between two nodes, the load is distributed to the two nodes using the cubic shape functions for the beam elements.

From the discrete time series of the load in each node, the load spectrum in the frequency-domain is found by Fourier transformation.

### 3.2 Modelling the track-embankment system

The numerical models presented in Figure 2 are constructed using 500 macro finite elements along the track. These macro finite elements describe the combined track, embankment and subsoil between two nodes along the track as illustrated in Figure 4. The spacing distance of the nodes in the finite element model equals the distance of 0.67 m between the railway sleepers at Ledsgaard, leading to a total length of 335 m in the numerical models. The out-of-plane degrees of freedom in the bottom part of the macro finite elements, introduced due to the three-dimensional soil modelling, are not considered in the modelling of the track-embankment system.

Thus, vibration in the lateral direction is not accounted for.

The individual beam elements in the macro finite element is modelled as either a Euler-Bernoulli beam or a Timoshenko beam. The governing partial differential equation for the Euler-Bernoulli beam is

$$q = EI_y \frac{\partial^4 u_z}{\partial x^4} + \rho A \frac{\partial^2 u_z}{\partial t^2} \quad (4)$$

where  $q$  is the force per unit length  $x$ ,  $E$  is Young's modulus,  $I_y$  is the second moment of area around the  $y$ -axis,  $\rho$  is the mass density,  $A$  is the cross-sectional area,  $t$  is time and  $u_z$  is the vertical displacement. The governing equations for the Timoshenko beam elements are the coupled linear partial differential equations given as

$$\rho A \frac{\partial^2 u_z}{\partial t^2} = q + \frac{\partial}{\partial x} \left[ k_s AG \left( \frac{\partial u_z}{\partial x} - \varphi \right) \right] \quad (5a)$$

$$\rho I_y \frac{\partial^2 \varphi}{\partial t^2} = EI_y \frac{\partial^2 \varphi}{\partial x^2} + k_s AG \left( \frac{\partial u_z}{\partial x} - \varphi \right) \quad (5b)$$

where  $k_s$  is the Timoshenko shear coefficient,  $G$  is the shear modulus and  $\varphi$  is the angular displacement or cross-sectional rotation.

Using the Galerkin approach, these governing partial differential equations are rewritten into finite-element form. The stiffness and mass matrices  $\mathbf{K}$  and  $\mathbf{M}$ , respectively, for the beam elements are given by the well known solutions for a complete two-dimensional element,

$$\mathbf{K} = \text{function}(L, E, A, \nu, k_s, I_y)$$

$$\mathbf{M} = \text{function}(L, \rho, A, I_y)$$

where  $L$  is the length of the element. In the case of a Euler-Bernoulli beam, the parameters  $\nu$  and  $k_s$  are not relevant.

In model three the embankment is modelled with continuum finite elements, and the governing partial

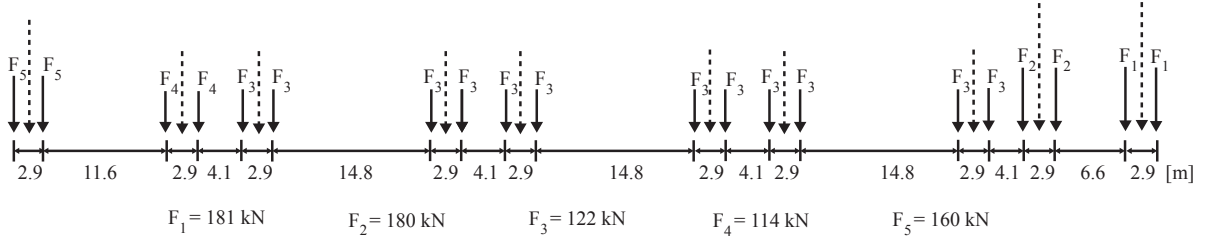


Figure 3: Axle distances and loads of the X2000 passenger train used at the test programme at Ledsgaard; (—) axle loads, (---) bogie loads.

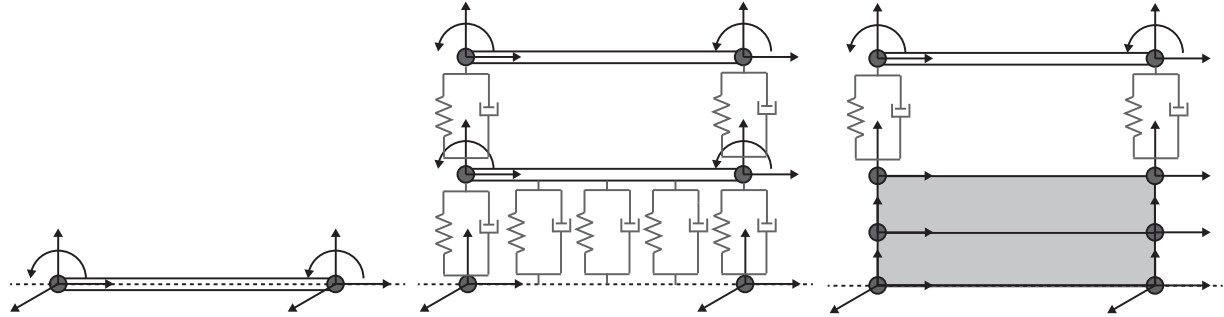


Figure 4: The macro elements used for the numerical modeling.

differential equation for the continuum is

$$\frac{\partial \sigma_{xx}}{\partial x} + \frac{\partial \sigma_{yx}}{\partial y} + \frac{\partial \sigma_{zx}}{\partial z} + \rho b_x = \rho \frac{\partial^2 u_x}{\partial t^2} \quad (6a)$$

$$\frac{\partial \sigma_{xy}}{\partial x} + \frac{\partial \sigma_{yy}}{\partial y} + \frac{\partial \sigma_{zy}}{\partial z} + \rho b_y = \rho \frac{\partial^2 u_y}{\partial t^2} \quad (6b)$$

$$\frac{\partial \sigma_{xz}}{\partial x} + \frac{\partial \sigma_{yz}}{\partial y} + \frac{\partial \sigma_{zz}}{\partial z} + \rho b_z = \rho \frac{\partial^2 u_z}{\partial t^2} \quad (6c)$$

Through multiplication with a virtual displacement field and integration over the volume, the stiffness and mass matrices for the finite element modelling of the embankment in model three are found by numerical (Gauss quadrature) evaluation of the integrals,

$$\mathbf{K} = \int_A \mathbf{B}^T \mathbf{D} t(z) \mathbf{B} dA \quad (7)$$

$$\mathbf{M} = \int_A \mathbf{N}^T \rho t(z) \mathbf{N} dA \quad (8)$$

where  $\mathbf{N}$  are the shape functions,  $\mathbf{B}$  is the differentiated shape functions,  $\mathbf{D}$  is the constitutive relation and  $t$  is the thickness of the element (i.e. the width of the embankment) which varies over the depth, cf. Figure 5.

The coupling between the rails and the embankment in model two and three consists of a discrete spring-damper system modelling the sleepers. A continuous spring/damper system coupling the embankment and the soil is used in model two. The horizontal stiffness along the track and the vertical stiffness in the spring system is approximated using,

$$k_h = \frac{GA}{w} \quad , \quad k_v = \frac{EA}{h}.$$

In the coupling between the rails and the embankment  $E$  and  $G$  are material parameters for the sleeper and  $A$  is the cross-sectional area,  $h$  is the height and  $w$  is the width of the sleeper. In the coupling between the embankment and the soil,  $E$  and  $G$  are material parameters for the embankment,  $h$  is the height of the embankment,  $w$  is the distance between the sleepers and  $A$  is the average cross-sectional areal of the embankment, calculated as the height of the embankment times the average width given as section AA in Figure 5.

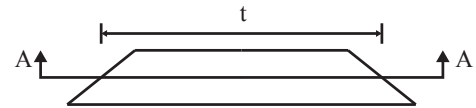


Figure 5: Cross-section of the embankment.

For all elements in the macro finite element the damping is introduced as structural damping proportional to the stiffness of the element,

$$\mathbf{C} = \alpha \mathbf{K}. \quad (9)$$

The matrices are obtained for each element in the track-embankment system and added to the global dynamic stiffness matrix,  $\tilde{\mathbf{K}}(\omega)$ .

### 3.3 Modelling the soil

The finite element model of the track-embankment system interacts with an elastic half-space representing the soil. The two systems are connected through a series of coupling points along the ground surface under the embankment. Discrete Green's functions are used to derive a dynamic flexibility matrix for

the coupling points. The dynamic flexibility matrix describes the wave field in the radial, transverse and vertical directions as functions of the frequency and distance from the source point to the observation point. The methodology used for calculating the Green's function was first proposed by Kausel and Roësset (1981). It combines integration in the frequency-wavenumber domain with the description of layered soils by transfer matrix methods, first given by Thomson (1950) and Haskell (1953).

The advantage of the frequency-wavenumber domain is that, for a given set of horizontal wavenumbers  $k_x$  and  $k_y$  and circular frequency  $\omega$  the displacement amplitudes  $\hat{\bar{U}}_i$  in the transformed domain are related directly to the traction amplitudes  $\hat{\bar{P}}_j$  as,

$$\hat{\bar{U}}_i(k_x, k_y, \omega) = \hat{\bar{G}}_{ij}(k_x, k_y, \omega) \hat{\bar{P}}_j(k_x, k_y, \omega) \quad (10)$$

where  $\hat{\bar{G}}_{ij}$  is the Green's function tensor.

The Green's function tensor is obtained using the Cauchy equation of motion revealed in Equation (6) but without considering the body forces. By application of Fourier transforms with respect to the coordinates  $x$ ,  $y$  and  $t$ , the partial differential equations of motion in each soil layer are reduced to ordinary differential equations in the vertical direction,

$$(\underline{\lambda} + \underline{\mu}) ik_x \underline{\Delta} + \underline{\mu} \left( \frac{d^2}{dz^2} - k_x^2 - k_y^2 \right) \hat{\bar{U}}_x = -\omega \rho \hat{\bar{U}}_x \quad (11a)$$

$$(\underline{\lambda} + \underline{\mu}) ik_y \underline{\Delta} + \underline{\mu} \left( \frac{d^2}{dz^2} - k_x^2 - k_y^2 \right) \hat{\bar{U}}_y = -\omega \rho \hat{\bar{U}}_y \quad (11b)$$

$$(\underline{\lambda} + \underline{\mu}) \frac{d\underline{\Delta}}{dz} + \underline{\mu} \left( \frac{d^2}{dz^2} - k_x^2 - k_y^2 \right) \hat{\bar{U}}_z = -\omega \rho \hat{\bar{U}}_z \quad (11c)$$

where the underline indicates the individual layers and  $\underline{\Delta} = \underline{\Delta}(k_x, k_y, z, \omega)$  is the double Fourier transform of the dilation amplitudes  $\underline{\Delta}(x, y, z, \omega)$ . The ordinary differential equation is solved imposing compatibility in vertical displacement and stress by appropriate boundary conditions at the free surface and layer interfaces. Soils are highly nonlinear materials, but in order to utilize the Fourier transformation a linear response is assumed.

The derivation of the Green's function tensor is based on an assumption of linear elastic, homogeneous and isotropic material within each soil layer. Evaluation of the Green's functions in the transformed space involves integration in the wavenumber domain corresponding to the coordinates  $k_x$ ,  $k_y$  and  $\omega$ . It is required that the Fourier transformed spatial field is described with satisfactory accuracy in the wavenumber domain in order to capture the local peaks in the Green's function corresponding to waves propagating in the soil. The Green's functions are evaluated along a single wavenumber axis in the

computations and the wavenumber step is controlled such that the average value between two wavenumbers differ less than 1% from the real value. In the evaluation, a combination of hysteretic and linear viscous damping is taken into account by using the loss factor  $\eta$  and introduce complex values for the Lamé constants,

$$\mu(\omega) = \frac{E(1 + i(\text{sign}\eta + \frac{\eta\omega}{2\pi 100}))}{2(1+\nu)} \\ \lambda(\omega) = 2\mu(\omega) \frac{\nu}{1-2\nu}$$

implying that the hysteretic damping and linear viscous damping are equal at 100 Hz.

The load from the train is transferred to the soil through the coupling points to the embankment. To establish the solution for the displacements in the transformed domain, the surface traction must also be transformed to the wavenumber domain. A Gaussian distribution of the load is used, leading to a bell-shaped load on the surface of the half-space. This situation is illustrated in Figure 6. The stan-

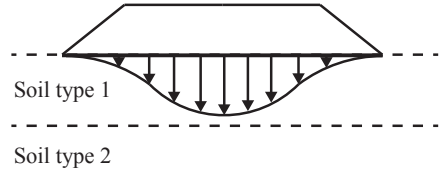


Figure 6: Distribution of the load under the embankment.

dard deviation for this Gaussian distribution is set to 1/6 of the width of the embankment, leading to a coverage of 99.73% of the load within the width of the embankment. The traction in Equation (10) is applied in the form

$$\hat{\bar{P}}_j(k_x, k_y, \omega) = \hat{D}(k_x, k_y) \tilde{P}_j(\omega) \quad (12)$$

where  $\hat{D}(k_x, k_y)$  is a distributed load with total magnitude 1. Hence the flexibility matrix in spatial domain is obtained by inverse Fourier transformation:

$$\tilde{G}_{ij}(x, y, \omega) = \frac{1}{4\pi^2} \int_{-\infty}^{\infty} \int_{-\infty}^{\infty} \hat{\bar{G}}_{ij}(k_x, k_y) \\ \times \hat{D}(k_x, k_y) e^{i(k_x x + k_y y)} dk_x dk_y. \quad (13)$$

For the bell-shaped load, the distribution is described by

$$\hat{D}(k_x, k_y) = e^{-(k_x^2 + k_y^2)^2 r_0^2} \quad (14)$$

in the wavenumber-domain. By inverting the flexibility matrix, the complex stiffness matrix of the soil is obtained,

$$\tilde{\mathbf{H}}(\omega) = \tilde{\mathbf{G}}(x, y, \omega)^{-1}, \quad (15)$$

where the components of  $\tilde{\mathbf{G}}$  are given by Equation (13). The complex stiffness matrix can be put into the finite element formulation of the numerical model in Equation (3) by the principle of standard finite element assembly.

## 4 Numerical simulations

The numerical model is used for simulations of 10 different train speeds in order to investigate when the dynamic effects are introduced. The response for the 10 train speeds is simulated in each of the three numerical models. Furthermore, the load is modelled in three different ways: as axle loads, as bogie loads and as a single bogie load. Thus, the number of simulations is 90. The case of a single bogie load is to examine if the dynamic effects are introduced in the same manner as if the entire train is modelled. The soil profile at Ledsgaard is approximated using five soil layers, the parameters of which are given in Table 1.

Table 1: Parameters for the soil.

		Value	Unit
<b>Layer 1 - crust</b>			
Height	$h$	1.1	m
Young's modulus	$E$	$11.58 \cdot 10^6$	Pa
Poisson's ratio	$\nu$	0.49	[ $\cdot$ ]
Damping coefficient	$\eta$	0.04	[ $\cdot$ ]
Mass density	$\rho$	1500	kg/m <sup>3</sup>
<b>Layer 2 - organic clay</b>			
Height	$h$	3.0	m
Young's modulus	$E$	$3.17 \cdot 10^6$	Pa
Poisson's ratio	$\nu$	0.49	[ $\cdot$ ]
Damping coefficient	$\eta$	0.02	[ $\cdot$ ]
Mass density	$\rho$	1260	kg/m <sup>3</sup>
<b>Layer 3 - clay</b>			
Height	$h$	4.5	m
Young's modulus	$E$	$9.34 \cdot 10^6$	Pa
Poisson's ratio	$\nu$	0.49	[ $\cdot$ ]
Damping coefficient	$\eta$	0.05	[ $\cdot$ ]
Density	$\rho$	1475	kg/m <sup>3</sup>
<b>Layer 4 - clay</b>			
Height	$h$	6.0	m
Young's modulus	$E$	$16.73 \cdot 10^6$	Pa
Poisson's ratio	$\nu$	0.49	[ $\cdot$ ]
Damping coefficient	$\eta$	0.05	[ $\cdot$ ]
Mass density	$\rho$	1475	kg/m <sup>3</sup>
<b>Layer 5 - clay</b>			
Height	$h$	-	m
Young's modulus	$E$	$22.09 \cdot 10^6$	Pa
Poisson's ratio	$\nu$	0.49	[ $\cdot$ ]
Damping coefficient	$\eta$	0.05	[ $\cdot$ ]
Mass density	$\rho$	1475	kg/m <sup>3</sup>

The parameters used for modelling the system on top of the ground are specified in Table 2.

Table 2: Parameters for the track-embankment system.

		Value	Unit
<b>Model 1 - track/embankment</b>			
Cross-sectional area	$A$	10.15	m <sup>2</sup>
Young's modulus	$E$	$100 \cdot 10^6$	Pa
Bending stiffness	$EI_y$	$80 \cdot 10^6$	Nm <sup>2</sup>
Mass density	$\rho$	1800	kg/m <sup>3</sup>
Damping coefficient	$\alpha$	0.01	[ $\cdot$ ]
<b>Model 2 and 3 - rail</b>			
Cross-sectional area	$A$	$7.67 \cdot 10^{-3}$	m <sup>2</sup>
Young's Modulus	$E$	$210 \cdot 10^9$	Pa
Bending stiffness	$EI_y$	$6.38 \cdot 10^{-6}$	Nm <sup>2</sup>
Mass density	$\rho$	7850	kg/m <sup>3</sup>
Damping coefficient	$\alpha$	0.01	[ $\cdot$ ]
<b>Model 2 and 3 - sleeper</b>			
Horizontal stiffness	$k_h$	$18.75 \cdot 10^9$	N/m
Vertical stiffness	$k_v$	$63.00 \cdot 10^9$	N/m
Damping coefficient	$\alpha$	0.01	[ $\cdot$ ]
<b>Model 2 - embankment</b>			
Cross-sectional area	$A$	10.15	m <sup>2</sup>
Young's modulus	$E$	$100 \cdot 10^6$	Pa
Bending stiffness	$EI_y$	$80 \cdot 10^6$	Nm <sup>2</sup>
Poisson's ratio	$\nu$	0.3	[ $\cdot$ ]
Shear correction factor	$k_s$	0.85	[ $\cdot$ ]
Mass density	$\rho$	1800	kg/m <sup>3</sup>
Damping coefficient	$\alpha$	0.01	[ $\cdot$ ]
<b>Model 2 - embankment-ground coupling</b>			
Horizontal stiffness	$k_h$	$0.46 \cdot 10^9$	N/m
Vertical stiffness	$k_v$	$0.38 \cdot 10^9$	N/m
Damping coefficient	$\alpha$	0.01	[ $\cdot$ ]
<b>Model 3 - embankment</b>			
Height	$h$	1.4	m
Width (top)	$w$	5.5	m
Width (bottom)	$w$	9	m
Young's modulus	$E$	$100 \cdot 10^6$	Pa
Poisson's ratio	$\nu$	0.3	[ $\cdot$ ]
Mass density	$\rho$	1800	kg/m <sup>3</sup>
Damping coefficient	$\alpha$	0.01	[ $\cdot$ ]

The numerical models are solved in the frequency range 0 - 30 Hz, due to observations in some pre-simulations, which indicated that the reponse of the soil were located below a frequency of 30 Hz. Figure 7 illustrates the track motion along the track for different train speeds simulated using the three different models and bogie loads as well as axle loads. From the figure it is observed that the reponse of model one and model two is identical. The difference between modelling the train as bogie or axle loads are restricted to a difference in the amplitude, since the pattern is identical. Furthermore, it is observed that model three in general underestimates the amplitudes. Actually, the reponse in model three is static for all the train speeds except 280 km/h, in contrast to model one and two which has dynamic response at speeds above 120 km/h. For models one and two it is clearly seen from the figure that the

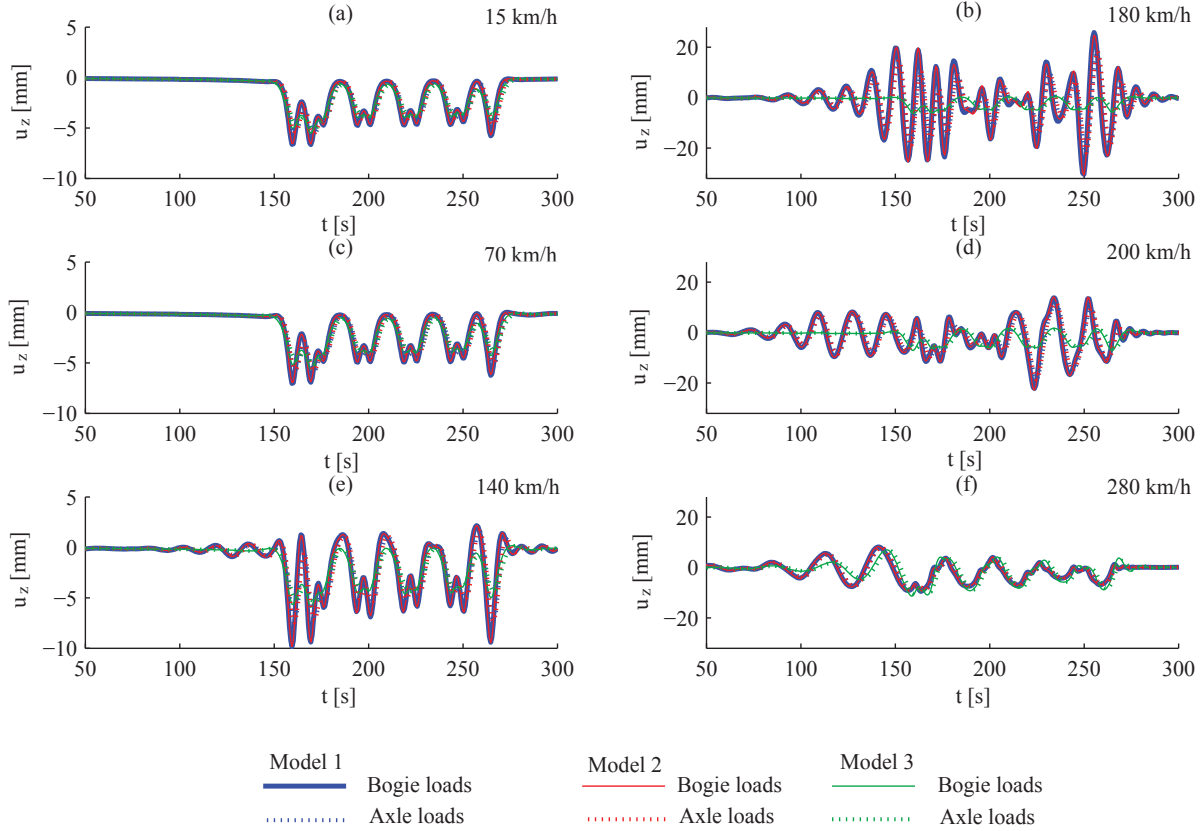


Figure 7: Snapshots of the train along the track.

response is static due to the low train speeds and as the train speed increases the reponse becomes dynamic. The position of the train along the railway track is the same for all train speeds. The instant position of the train loads is easily identified for the low train speeds, but for the high train speeds the position of the train loads are hard to identify. The figures also show that for the dynamic response, the tail of free oscillations are present in the range 50 - 100 m behind the train.

The response for a train speed of 70 km/h at the node located at  $y = 235$  m is illustrated in Figure 8. Figure 8a and 8c illustrate the load time series and the displacement time series, respectively. Figures 8b and 8d are corresponding to Figure 8a and 8c where there has been zoomed on the time series where the train passes the node. Figure 8e illustrates the frequency spectrum of the displacement response. The same graphs are illustrated in Figure 9 for a train speed of 200 km/h.

Obviously some of the same observations is made as in Figure 7. Model three underestimates the reponse, especially at high train speeds. There is no significant difference between models one and two. The difference between modelling the train as bogie loads or axle loads is in the displacement amplitude of the response. From Figures 8e and 9e it is clear that the response in the frequency domain tends

to higher frequencies as the train speed increases. Thus, at a train speed of 70 km/h the primary response is in the range 0 - 2 Hz and for a train speed of 200 km/h it is in the range 0 - 10 Hz and mostly in the range 2 - 4 Hz.

The data from the Ledsgaard site have been unavailable to the authors of the present paper, and that is the reason why Figures 8 and 9 are plotted for the speeds of 70 km/h and 200 km/h. These are mainly the plots presented by the papers cited in Section 2 and thus they provide the possibility to compare with the measurements from Ledsgaard presented in these papers. The pattern of response agrees well with the measurements from Ledsgaard for models one and two, unlike model three which does not capture the dynamic effects at the high train speeds. At low train speed the amplitudes of the response agrees well with the measurements, however at the high train speeds the models overestimate the displacement amplitudes. The measurements at Ledsgaard show a displacement range from 0 to -6 mm in the case of a train speed of 70 km/h and in the range from 6 to -15 mm in the case of a train speed of 200 km/h. This corresponds to an increase of the peak-to-peak amplitude with a factor of 3.5. This dynamic amplification for the simulation models is shown in Figure 10b. Figure 10a illustrates the change in positive and negative

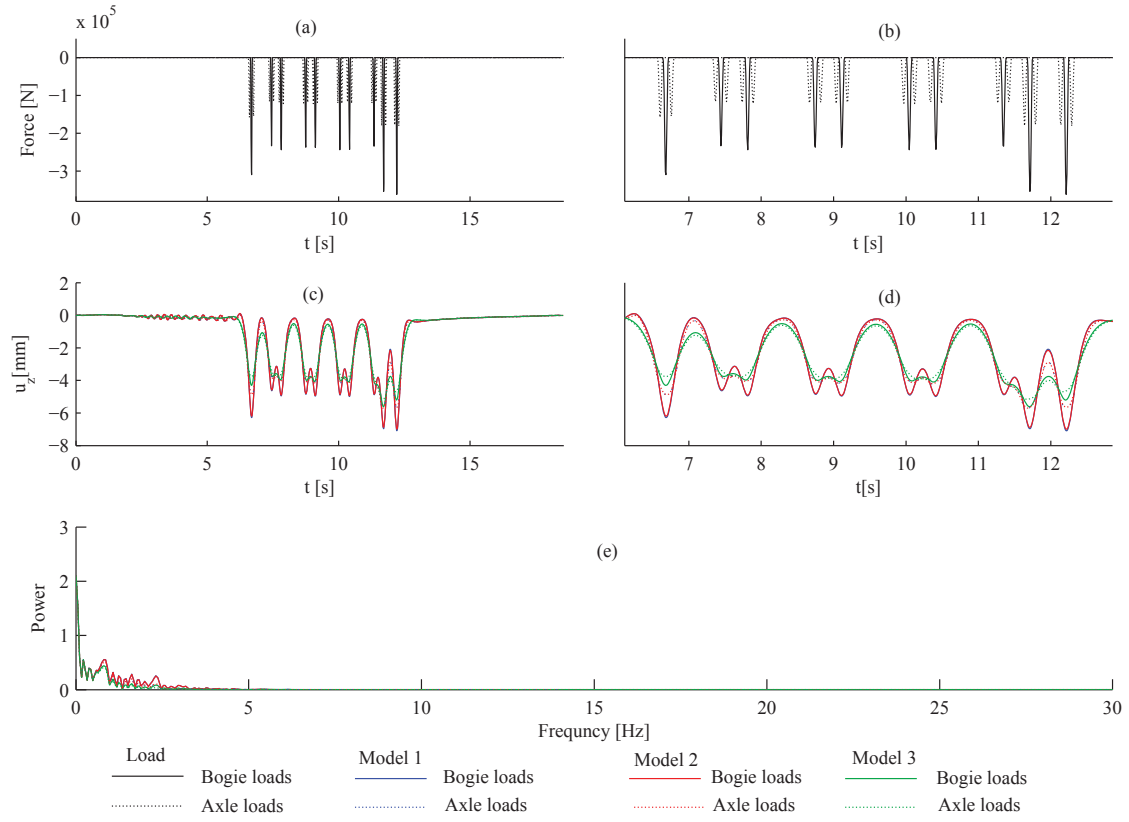


Figure 8: Response in a point on the track at a train speed of 70 km/h.

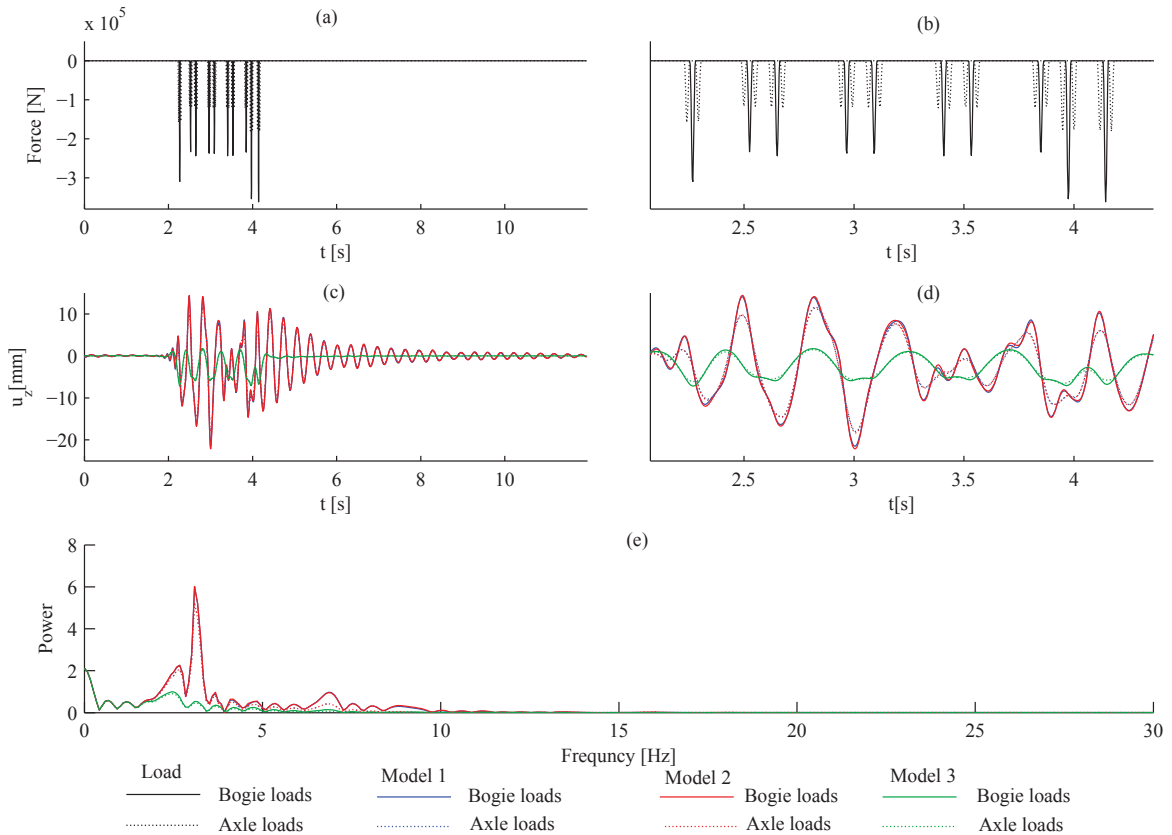


Figure 9: Response in a point on the track at a train speed of 200 km/h.

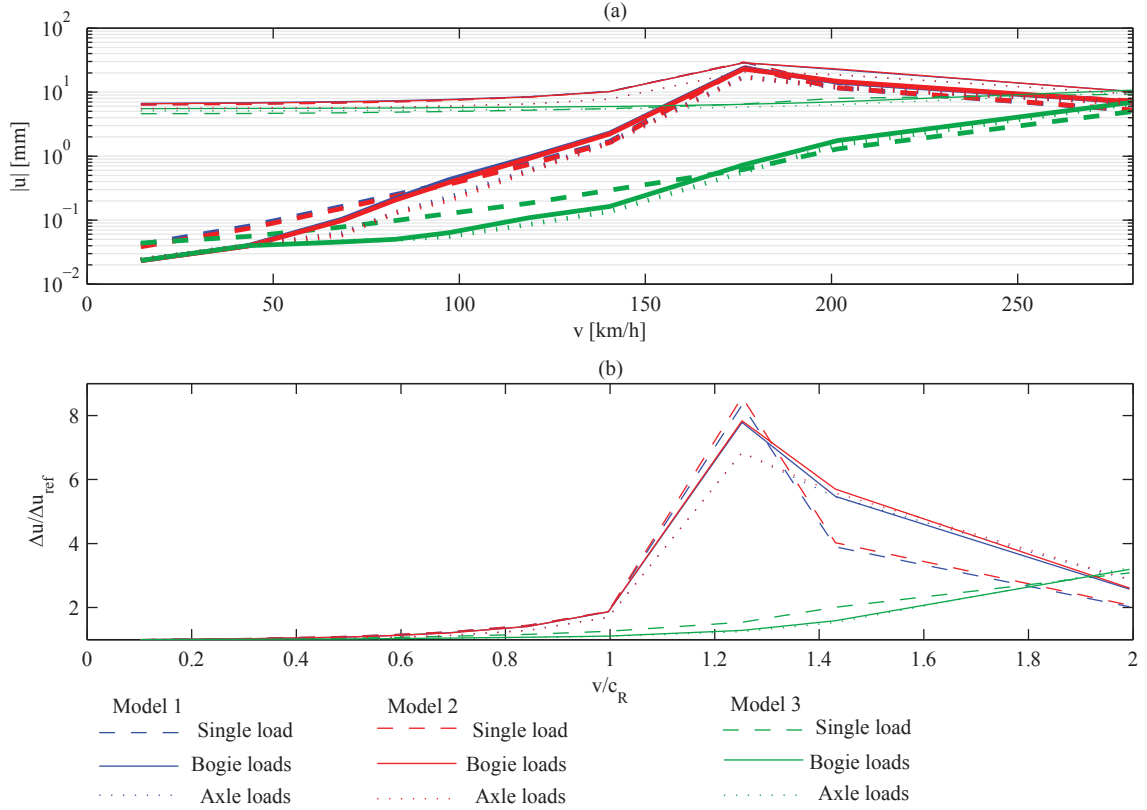


Figure 10: Dynamic amplification as function of increasing train speed. (a) absolute value of the displacement in downward (thin lines) and upward direction (thick lines), (b) peak-to-peak displacements normalized with the static peak-to-peak displacement as function of the train speed relative to the Rayleigh wave propagation speed in the second soil layer.

displacement amplitude due to increase in the train speed. It is observed that it is the positive amplitude which increases dramatically due to increase in the train speed and this is also observed in Figure 7. At a train speed of 280 km/h the positive amplitudes has become almost the same at the negative amplitude. This implies a nearly harmonic response where the negative amplitude is higher due to the weight of the train. From the figure it is seen that the difference between model one and two with bogie or axle loads are almost negligible. This is more clearly observed in Figure 10b where the four corresponding lines are closely related. From this figure it is evident that the dynamic effects introduced in model one and two with bogie or axle loads are also reproduced if only a single load is moving along the railway. This means that in investigations of the critical speed the modelling of the load is a secondary parameter. However, the factor of dynamic amplification and, obviously, the displacement response are not predicted in an identical manner.

It is generally recognized that the critical speed, i.e. the point of dramatical increase in Figure 10b, for a homogeneous half-space is directly related to the Rayleigh wave speed of the material. The wave speeds in this numerical simulation are given in Table 3.

Table 3: Phase speeds of wave propagation.

		Soil layer				
		1	2	3	4	5
$c_P$	km/h	1800	1800	5400	5400	5400
$c_S$	km/h	259	148	234	313	360
$c_R$	km/h	247	141	223	299	344

From Figure 10b is it shown that the critical speed is around 180 km/h. This critical speed is hard to identify from Table 3, thus the critical speed may not be predictable by information regarding the wave speeds in the individual soil layers. The critical speed is somehow a combination depending on the wave speeds in the individual layers, the height of the layer and the order of them. A more precise prediction may be obtained using dispersion diagrams. The dispersion diagrams related to the soil profile used to represent the Ledsgaard site in the numerical simulations are shown in Figure 11.

From Figure 7b the simulation with a speed of 180 km/h has the highest dynamic effects and the line corresponding to this speed is illustrated in Figure 11. It then becomes evident why this speed causes the highest dynamic response. The line of the train speed crosses and afterwards follows the curve of the high amplitude in the dispersion diagrams, i.e.

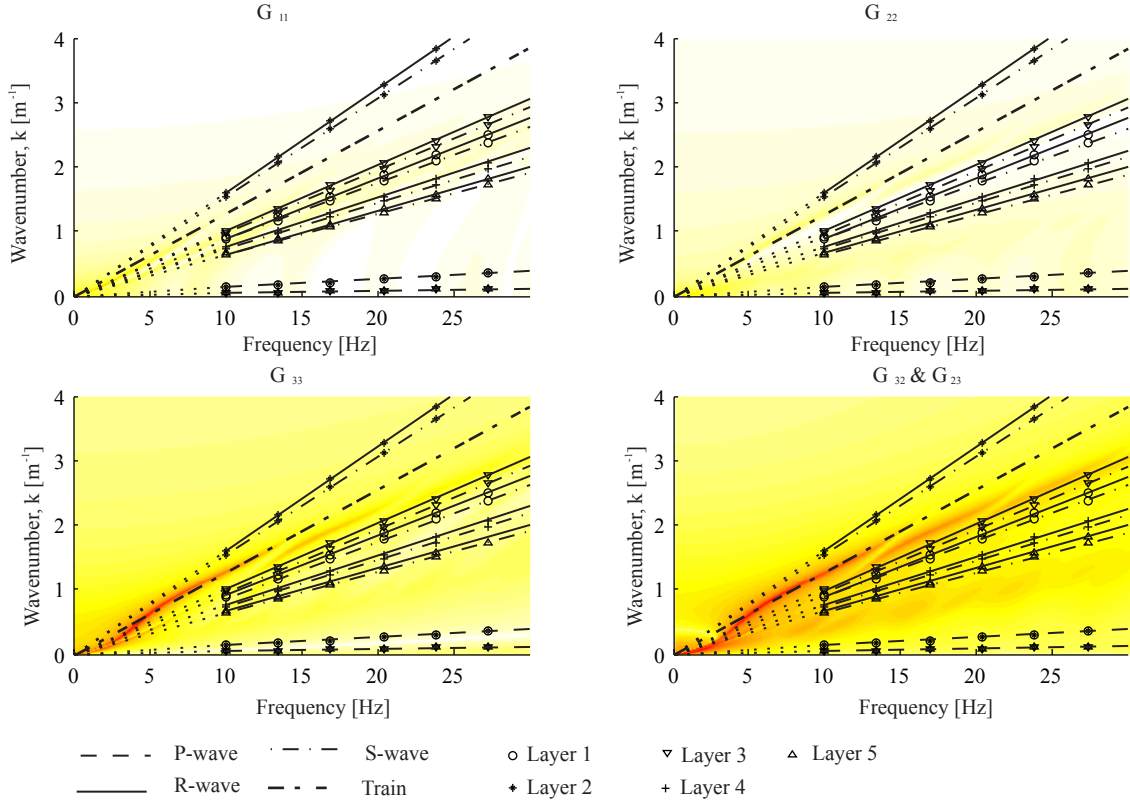


Figure 11: Dispersion diagrams with dispersion curves for P, S and Rayleigh (R) waves in layer 1-5 and for the train speed 180 km/h. Dark red colours indicate high response levels.

a speed of 180 km/h excites the critical combination of frequency and wavenumber in the ground. From Figure 9e it is observed that the frequency spectrum of the response for a train speed of 180 km/h is in the range of 0 - 10 Hz highly concentrated in the range 2 - 4 Hz. This is consistent with the observation in Figure 11c and 11d, where the peak amplitude fades out around 10 Hz and the crossing of the peak amplitude is in the region of 5 Hz. Thus, it is possible to identify the critical speed from the dispersion diagrams, i.e. the train speeds should form a dispersion curve which does not cross or follow the dispersion curves for wave propagation in the system.

## 5 Conclusion

This paper presented three models to simulate the dynamic amplifications of deformations in railways due to high-speed trains on soft ground. In all three models the ground is modelled as a layered half-space. In the first model, the track-embankment system is modelled as a Euler-Bernoulli beam. In the second model, the rail is still modelled as a Euler-Bernoulli beam, but the embankment is modelled as a Timoshenko beam. The coupling between the two beams is a spring/damper system with the property as a railway sleeper. The coupling between the embankment and the ground is modelled as a

consistent spring/damper system. In the third model, the rail is modelled as a Euler-Bernoulli beam and the embankment as continuum finite elements with the same coupling as the second model. To validate the model, the Ledsgaard case from Sweden is used. The Ledsgaard case is a site on the railway line between Malmö and Gothenburg in Sweden, where a velocity upgrade in 1997 caused a significant increase in the vibrations of the surrounding soil and a large study with appurtenant measurements was performed. Simulations are performed with the three models with the train load modelled as a single load, bogie loads and axle loads. The two first models give almost equal results, where the third model gives results smaller than the two others. Compared with the measurements from Ledsgaard the first two models overestimating the displacement amplitudes where the third model leads to an underestimation. The third model does not establish the dynamic amplification, where the two first models perform very well. All three methods to model the train loads establish the dynamic amplification but give a difference in the displacements. Hence, it may be concluded that the simple model with the track and embankment modelled as a single beam can be used. However, the full pattern of axle loads must be accounted for.

## References

- Adolfsson, Andréasson, Bengtsson, and Zackrisson, 1999.** K. Adolfsson, B. Andréasson, P. Bengtsson, and P. Zackrisson. *High speed train X2000 on soft organic clay - measurements in Sweden*. Geotechnical Engineering for Transportation Infrastructure, 3, 1713–1718, 1999.
- Andersen and Nielsen, 2003.** L. Andersen and S.R.K. Nielsen. *Boundary element analysis of the steady-state response of an elastic half-space to a moving force on its surface*. Engineering Analysis with Boundary Elements, 27, 23–38, 2003.
- Andersen, Nielsen, and Kirkegaard, 2001.** L. Andersen, S.R.K. Nielsen, and P.H. Kirkegaard. *Finite element modelling of infinite Euler beams on Kelvin foundations exposed to moving loads in convected co-ordinates*. Journal of Sound and Vibration, 241, 587–604, 2001.
- Andersen, 2006.** L.A. Andersen. *Linear Elastodynamic Analysis*, 2006.
- Ballard, 2010.** M.S. Ballard. *Doppler effect*. The Journal of the Acoustical Society of America, 127, p. 1912, 2010.
- Bathe, 2007.** K.J. Bathe. *Finite element procedures*. Klaus-Jurgen Bathe, 2007. ISBN 978-097-900-490-2.
- Beskos and Manolis, 1988.** D.E. Beskos and G.D. Manolis. *Boundary element methods in elastodynamics*. Unwin Hyman, 1988. ISBN 978-004-620-019-0.
- Bettess, 1992.** P. Bettess. *Infinite elements*. Penshaw Press, 1992. ISBN 978-095-188-060-9.
- Cook, Malkus, Plesha, and Witt, 2001.** R.D. Cook, D.S. Malkus, M.E. Plesha, and R.J. Witt. *Concepts and applications of finite element analysis*. John Wiley, 2001. ISBN 978-047-135-605-9.
- Costa, Calcada, Cardoso, and Bodare, 2010.** P.A. Costa, R. Calcada, A.S. Cardoso, and A. Bodare. *Influence of soil non-linearity on the dynamic response of high-speed railway tracks*. Soil Dynamics and Earthquake Engineering, 30, 221–235, 2010.
- Dieterman and Metrikine, 1996.** H.A. Dieterman and A. Metrikine. *The equivalent stiffness of a half-space interacting with a beam. Critical velocities of a moving load along the beam*. European Journal of Mechanics, 15, 67–90, 1996.
- Dominguez, 1993.** J. Dominguez. *Boundary elements in dynamics*. Computational Mechanics, 1993. ISBN 978-185-312-258-3.
- Galvín and Domínguez, 2007.** P. Galvín and J. Domínguez. *Analysis of ground motion due to moving surface loads induced by high-speed trains*. Engineering Analysis with Boundary Elements, 31, 931–941, 2007.
- Haskell, 1953.** N.A. Haskell. *The dispersion of surface waves on multilayer media*. Bulletin of the Seismological Society of America, 43, 17–34, 1953.
- Jernbanen.dk.** Jernbanen.dk. *SJS Damplokotivier*. <http://www.jernbanen.dk>. Visited on 26/05/2014.
- Karlström and Boström, 2006.** A. Karlström and A. Boström. *An analytical model for train-induced ground vibrations from railways*. Journal of Sound and Vibration, 292, 221–241, 2006.
- Kausel and Roësset, 1981.** E. Kausel and J.M. Roësset. *Stiffness matrices for layered soils*. Bulletin of the Seismological Society of America, 71, 1743–1761, 1981.
- Kaynia, Madshus, and Zackrisson, 2000.** A.M. Kaynia, C. Madshus, and P. Zackrisson. *Ground Vibration from High-Speed Trains: Prediction and Countermeasure*. Journal of Geotechnical and Geoenvironmental Engineering, 126, 531–537, 2000.
- Krylov, 1995.** V.V. Krylov. *Generation of Ground Vibrations by Superfast Trains*. Applied Acoustics, 44, 149–164, 1995.
- Madshus and Kaynia, 2000.** C. Madshus and A.M. Kaynia. *High-speed railway lines on soft ground: Dynamic behaviour at critical train speed*. Journal of Sound and Vibration, 231, 689–701, 2000.
- Paolucci, Maffei, Scandella, Stupazzini, and Vanini, 2003.** R. Paolucci, A. Maffei, L. Scandella, M. Stupazzini, and M. Vanini. *Numerical prediction of low-frequency ground vibrations induced by high-speed trains at Ledsgaard, Sweden*. Soil Dynamics and Earthquake Engineering, 23, 425–433, 2003.
- Sheng, Jones, and Petyt, 1999.** X. Sheng, C.J.C. Jones, and M. Petyt. *Ground vibration generated by a harmonic load acting on a railway track*. Journal of Sound and Vibration, 225, 3–28, 1999.
- Takemiya, 2003.** H. Takemiya. *Simulation of track-ground vibrations due to a high-speed train: the case of X-2000 at Ledsgard*. Journal of Sound and Vibration, 261, 503–526, 2003.
- Thomson, 1950.** W.T. Thomson. *Transmission of elastic waves through a stratified soil medium*. Journal of Applied Physics, 21, 89–93, 1950.
- Woldringh and New, 1999.** R.F. Woldringh and B.M. New. *Embankment design for high speed trains on soft soils*. Geotechnical Engineering for Transportation Infrastructure, 3, 1703–1712, 1999.
- Wolf and Song, 1998.** J.P. Wolf and C. Song. *Consistent infinitesimal finite-element cell method in frequency domain*. Earthquake Engineering and Structural Dynamics, 25, 1307–1327, 1998.
- Zhenpeng, 2001.** L. Zhenpeng. *Transmitting boundary and radiation conditions at infinity*. Science in China Series E: Technological Science, 44, 177–186, 2001.
- Zienkiewicz, Taylor, and Zhu, 2005.** O.C. Zienkiewicz, R.L. Taylor, and J.Z. Zhu. *The finite element method: Its basis and fundamentals*. Elsevier Butterworth-Heinemann, 2005. ISBN 0-7506-6320-0.



# Article II



# Parameter study regarding dynamic amplification of deformations in railways due to high-speed traffic on soft ground

Andreas Elkjær Riis<sup>◦</sup> Søren Holm<sup>◦</sup>

Lars Vabbersgaard Andersen<sup>•</sup>

*Master students<sup>◦</sup> and associate professor<sup>•</sup> at  
Department of Civil Engineering, Aalborg University, Denmark*

---

## Abstract

The phenomenon of dynamic amplification of the displacement response has been observed at several locations as a result of increasing train speeds. The phenomenon is mainly restricted to locations with high-speed traffic on soft ground, where the speed of the train approaches the speed of the surface waves in the ground. A parameter study designed to identify the importance of the soil properties in the subsoil is performed. Individual soil parameters are studied as well as the stratification and the stiffness of the overlying embankment. The parameter study is based on a numerical model which models the track-embankment-subsoil system as a Euler-Bernoulli beam interacting with a layered half-space.

---

## 1 Introduction

The implementation of high-speed trains has enabled the possibility of implementing an one-hour model in the Danish railway traffic. The one-hour model is intended to ensure that the travelling time between the larger cities in Denmark does not exceed one hour. The railway lines included are Copenhagen-Odense, Odense-Aarhus, Aarhus-Aalborg and Odense-Esbjerg and today the train speed is in the range of 120-180 km/h on the referred railway lines. In order to be designated as high-speed trains, the speed of the train has to be at least 200 km/h.

A similar upgrade, at the Ledsgaard site on the railway line between Malmö and Gothenburg in Sweden, caused a significant increase in the vibrations of the surrounding soil, cf. Adolfsson et al. (1999). Due to the experience at Ledsgaard, the dynamic effects caused by high-speed trains is an important phenomenon to investigate. The phenomenon has environmental effects related with nuisance to people in buildings near the railway lines as well as structural consequences which may compromise the stability and safety. The worst-case scenario would be derailment of the train.

### 1.1 Observations and measurements

Due to the implementation of high-speed trains the study of railway vibrations has received increasing attention. However, the attention seems to be more

in the theoretical than the experimental part. Data from field measurements are hardly available in the literature, even though Woldringh and New (1999) report on a small amount of data of measurements conducted at three different sites.

At Stilton Fen in the United Kingdom measurement of the vertical deflections due to trains travelling at speeds in the range 130 to 180 km/h were conducted in 1993. The embankment consisted of ballast and ash to a depth of about 2.6 m and a thin layer of silty sand and gravel which overlies peat and very soft silty clay. The peak-to-peak deflections at relatively low speeds were 5 mm, whereas it was 12 mm at the highest speed.

At a specific location on the railway line between Amsterdam and Utrecht in the Netherlands similar measurements were conducted — here with train speeds in the range of 40 to 200 km/h on an embankment consisting of 2 m of sand fill over 6 m soft clay and peat layers. The peak-to-peak deflections were in the range 0.6 to 1.9 mm for the tested train speeds.

At the Ledsgaard site the testing was conducted at train speeds in the range 10 to 204 km/h. The embankment consisted of 1.4 m crushed bedrock and gravel underlayered by a 1.5 m dry weathered crust layer over a 3.0 m thick layer of soft organic clay. Under the soft organic clay a deposit of soft marine clay is present, having a thickness of more than 50 m and beneath this bedrock is present. In this case the peak-to-peak deflections were in the range of 6

to 17 mm.

From these test sites, it is obvious that increased vibration due to high-speed trains develop, which in this paper will be referred to as the dynamic effect. Unfortunately, the availability of data from field measurements are generally very limited, meaning that evaluating trends in the response from measurement is a challenging task. However, in order to clarify the phenomenon and understand the mechanism of the behaviour, measurements with varying train speeds are needed as well as investigations of the properties of the embankment and geotechnical conditions and the geodynamic properties of the soil materials. Thus, the investigations are comprehensive.

As can be seen from the data reported by Woldringh and New (1999) the dynamic effect of high train speeds is observed at all three locations, even at the location between Amsterdam and Utrecht where the deflections are rather small compared to the two other sites. The fact that the magnitude of the deflections are very different, even though the soil profile to some extent is quite similar, implies that the properties of the materials and the structure strongly influences the response of the structure and surrounding soil. The strong influence of the soil profile, the stiffness and the damping of the soil on the vibration levels is also recognized by Auersch (1994). Therefore, it may be impossible to predict the response at a given site from field measurements at a similar site. Thus, a mathematical model of the train-structure-soil interaction may actually be more beneficial.

In order to validate and calibrate such mathematical models the usage of field measurements would be a preferable tool. Eventhough the amount of data in general is limited, a comprehensive investigation was conducted in relation to the dynamic effects observed at Ledsgaard in Sweden. The investigations comprise a total of 20 test runs with different train speeds as well as determination of the material and geotechnical properties at the site. This data provides an unique opportunity to reproduce the phenomena through mathematical models.

From analysis of the data regarding the dynamic behavior of the system Madshus and Kaynia (2000) and Kaynia et al. (2000) came to the conclusion that the displacement field can be divided into two sub-parts, a quasi-static part and a dynamic part. The quasi-static field contains downward displacements due to the mass of the train simply moving with the load. The dynamic field contains displacements with equally upward and downward amplitudes and free oscillations follows behind the train.

## 1.2 Dynamic effects

The dynamic effects of the soil is due to wave propagation in the medium. Mainly three different waves

are usually encountered in the soil: primary waves, secondary waves and Rayleigh waves denoted P-waves, S-waves and R-waves, respectively. The P-waves are pressure waves, the S-waves are shear waves and the Rayleigh waves are a combination of pressure and shear waves propagating in the surface of the ground. The phase velocities of the wave types are

$$c_P = \sqrt{\frac{\lambda + 2\mu}{\rho}} , \quad c_S = \sqrt{\frac{\mu}{\rho}} , \quad (1)$$

$$c_R = \frac{0.87 + 1.12\nu}{1 + \nu} c_S ,$$

where  $\nu$  is the Poisson's ratio,  $\rho$  is the mass density, and  $\mu$  and  $\lambda$  are the Lamé constants. Since the Lamé constants are positive,  $c_P > c_S > c_R$ . In an isotropic, elastic material, and in a fixed frame of reference, the waves propagate at the characteristic speed in all directions.

Mixing of different wave types may take place in an interface between two soil layers or at a boundary. At a fixed or free boundary the waves are fully reflected into the indigenous material, and at a layer interface part of the energy is transmitted from one layer to another, and the remaining part of the energy is reflected. The relation between the transmitted and the reflected energy is described using the mechanical impedance of the two materials on either side of the interface. The mechanical impedance is given by

$$Z = \rho c$$

where  $\rho$  is the mass density and  $c$  is the phase speed of the wave. The transmission and reflection coefficient  $C_t$  and  $C_r$ , respectively, with regard to the particle velocities and displacements in two adjacent materials are given by

$$C_t = \frac{2}{1 + \frac{Z_2}{Z_1}} , \quad C_r = C_t - 1$$

The transmission and reflection coefficient, respectively, with regard to the energy in two adjacent materials are given by

$$E_t = \frac{Z_2}{Z_1} C_t^2 , \quad 1 = E_t + E_r$$

Obviously, all the energy is transmitted if  $Z_2/Z_1 = 1$  and consequently no energy is transmitted if  $Z_2/Z_1 \rightarrow 0$ . The main observation is, that the impedance mismatch between two materials is closely related to the transmission and reflection at the interface.

## 1.3 Mathematic model for parametric studies

The aim of this paper is to conduct a parametric study on which parameters are important in relation

to the dynamic effects of the response due to high-speed trains. The parametric study is performed using a numerical model to simulate the situation of a train moving along a railway track. In order to ensure selection of a reliable model, a literature study of models validated using the data from Ledsgaard is performed.

The simulations performed by Kaynia et al. (2000) and Paolucci et al. (2003) reproduces the measurements well regarding both pattern and amplitude. The situation is modelled as a beam interacting with a horizontally layered viscoelastic half-space and a beam interacting with an elastic foundation, respectively. The model by Kaynia et al. (2000) was developed further by Madshus and Kaynia (2000) to account for non-linear behaviour of the materials. The simulations, especially the pattern of response, agrees with the measurements. Karlström and Boström (2006) used a Euler-Bernoulli beam and an anisotropic Kirchhoff plate to model the rails and the sleepers, respectively. The embankment and the ground is modelled as viscoelastic materials. For low train speeds the simulations agree almost exactly, and in general a good agreement was observed. Inspired by Madshus and Kaynia (2000), the model developed by Costa et al. (2010) also takes the non-linearity into account. The rails are modelled as Euler-Bernoulli beams connected to the embankment via a spring/damper system forming the rail pads. The embankment and the ground is modelled using 2.5D finite elements. Investigation of the inclusion of the non-linearity was performed and showed that excluding the non-linearity underestimated the amplitudes while good agreement was observed when non-linearity was included. Also Takemiya (2003) included non-linearity in a model composing of a Euler-Bernoulli beam and a layered viscoelastic half-space. The agreement with measurement was much better at low train speeds compared to high train speeds. Based on this review it is very common to model the situation of a train moving along a railway track as a beam interacting with a half-space. The same approach was taken by Holm et al. (2014), however also two other models were investigated. The second model consisted of a Euler-Bernoulli beam representing the rail, a Timoshenko beam modelling the embankment and a layered half-space modelling the ground. The third model also uses a Euler-Bernoulli beam to model the rails and then 2D finite elements and a layered half-space to model the embankment and the ground, respectively.

The parametric study in this paper is performed adopting the first model by Holm et al. (2014), i.e. a model with a Euler-Bernoulli beam on top of a half-space. A detailed description of the model is given by Holm et al. (2014), while the main structure is summarised in Section 2. The aim of this paper is to study the importance of different parameters

regarding the amount of dynamic amplification as well as the point of introduction of the dynamic effects. The reference case in this parameter study is presented in Section 3 along with a pre-study investigating the performance of the model in order to ensure representative results. In Section 4.1 the importance of some of the soil parameters is studied. In section 4.2 the depth of the top-layer in a two-layered stratum is studied and in Section 4.3 the influence of the embankment stiffness is investigated. In general the parametric study is conducted for homogeneous half-spaces as well as two-layered half-spaces.

## 2 The simulation model

An overall illustration of the situation the numerical model is to analyse is given in Figure 1. The figure illustrates a train moving along a railway track supported by an embankment placed on the ground surface.

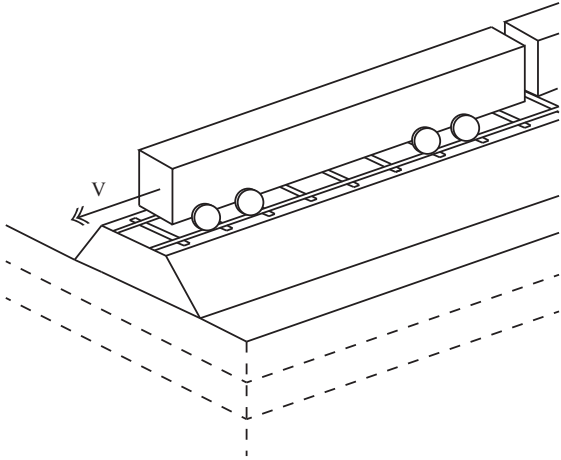


Figure 1: A part of the train moving along the railway system comprising the rails, embankment and the ground.

Numerically, the system is modelled using an ordinary finite-element (FE) formulation, i.e. characterizing it by a mass matrix, a damping matrix and a stiffness matrix.

The rails and the embankment are modelled as Euler-Bernoulli beam finite elements with translational degrees of freedom in the vertical and longitudinal direction as well as a rotational degree of freedom around the transverse direction. Thus, the stiffness and mass matrices of each element are given by the solution for a 2D Euler-Bernoulli beam element,

$$\mathbf{K} = \text{function}(L, E, A, I_y) \quad , \quad (2)$$

$$\mathbf{M} = \text{function}(L, \rho, A, I_y) \quad , \quad (3)$$

where  $L$  is the length,  $E$  the Young's modulus,  $\rho$  the mass density,  $A$  the cross-sectional area and  $I_y$

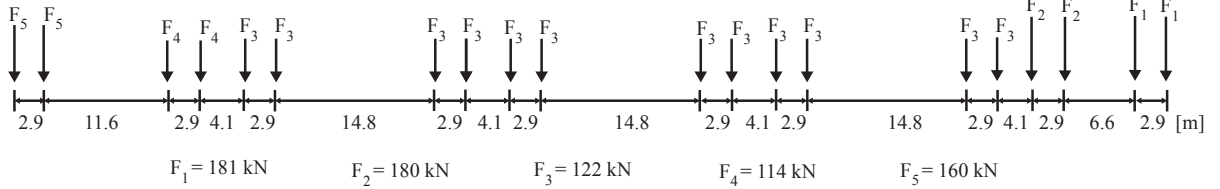


Figure 2: Axle distances and loads of the X2000 passenger train used at the test program at Ledsgaard.

the second moment of inertia of the beam element. The damping of the track-embankment system is introduced by a structural damping model, which provides damping proportional to the stiffness as

$$\mathbf{C} = \alpha \mathbf{K}, \quad (4)$$

where  $\alpha$  is a damping constant.

The soil is modelled using discrete Green's functions describing the flexibility of the soil, i.e. the wave field in the longitudinal, transverse and vertical directions. The embankment is connected to the ground through a number of points along the railway and these points coincide with the nodes in the modelling of the rail and embankment using beam elements. Thus, an extra degree of freedom is added in each node due to wave propagation in three dimensions. The discrete Green's functions are obtained by transforming the Cauchy equation of motion in each soil layer to an ordinary differential equation applying Fourier transformation with regard to the horizontal coordinates  $x$  and  $y$  and the time  $t$ . The ordinary differential equation is solved imposing compatibility in vertical displacement and stress by appropriate boundary conditions at the free surface and layer interfaces. The derivation of the Green's function tensor is based on an assumption of linear elastic, homogeneous and isotropic material within each soil layer. Application of the Fourier transformation implies that linear response is assumed.

The discrete Green's functions are assembled in a dynamic flexibility matrix. The application of Fourier transformation from the time domain to the frequency domain means that a complex dynamic flexibility matrix for the soil is obtained for each single frequency. Thus, the system is solved in the frequency domain. In order to do this, the stiffness, damping and mass of the track-embankment system is converted to a complex dynamic stiffness matrix by

$$\tilde{\mathbf{K}}(\omega) = -\omega^2 \mathbf{M} + i\mathbf{C} + \mathbf{K}. \quad (5)$$

Inverting the flexibility matrix of the soil it becomes an equivalent dynamic stiffness matrix, which can be combined with the dynamic stiffness matrix in Equation (5), and then the displacements of the sys-

tem in the frequency domain is solved using

$$\tilde{\mathbf{K}}(\omega) \tilde{\mathbf{U}}(\omega) = \tilde{\mathbf{F}}(\omega) \quad (6)$$

$$\tilde{\mathbf{K}}(\omega) = \begin{bmatrix} \tilde{\mathbf{K}}_{11}(\omega) & \tilde{\mathbf{K}}_{12}(\omega) \\ \tilde{\mathbf{K}}_{21}(\omega) & \tilde{\mathbf{K}}_{22}(\omega) + \tilde{\mathbf{H}}(\omega)^{-1} \end{bmatrix} \quad (7)$$

where  $\tilde{\mathbf{K}}_{11}$  refers to the rotational degrees of freedom in the system,  $\tilde{\mathbf{K}}_{22}$  refers to the translational degrees of freedom,  $\tilde{\mathbf{H}}(\omega_j)$  is the dynamic flexibility matrix of the soil and  $\tilde{\mathbf{F}}(\omega_j)$  is the Fourier transform of the discrete time series for the load. The time-domain solution of the discrete time series of the displacements is found using inverse Fourier transformation.

The discrete time series for the load is determined from a series of axle loads moving with constant speed along the railway track. In reality the forces consist of a quasi-static term due to the mass of the train moving along the railway and a dynamic term due to track irregularities and vehicle defects, e.g. wheel flats. In the analysis the train is decoupled from the track, implying that the interaction between the rails and the train is neglected. Furthermore, the dynamic term due to track irregularities and vehicle defects is omitted, thus the train is modelled as a series of constant loads moving with constant speed along the railway. For a visco-elastic half-space exposed to moving loads Yang and Hung (2009) studied the influence of the number of loads. It was observed that an increase in number of loads caused an increase in the displacement, whereas the velocity and acceleration of the soil remained unchanged. Holm et al. (2014) also studied this and found that the dynamic amplification is identified regardless of the number of loads. However, the displacement amplitude and, obviously, the response pattern depends on the number of loads.

In the present analysis the axle loads are modelled in accordance with the train used in the investigations at Ledsgaard in Sweden. The train consists of an engine and four cars, having a total length of approximately 109 m. The axle loads and spacing distances are illustrated in Figure 2.

The numerical model is constructed using 500 beam elements along the track meaning that the system has 2004 degrees of freedom. The length of the beam finite elements is 0.67 m which is equivalent

to the distance between the sleepers at the Ledsgaard site. Thus, the model has a total length of 335 m. When the axles are in a position between two nodes in the finite element system, the loads are distributed to the nodes using the cubic shape functions for the beam elements.

### 3 The reference case

A good practice in the case of a parameter study is to set up a reference case. Then the results after a change in a given parameter are compared with the results from the reference case and then the influence of the parameter can be evaluated.

In the numerical model the series of moving loads representing the moving train are decoupled from the track. Hence, the interaction between the train and the track-embankment structure is neglected. The numerical model is constructed using a Euler-Bernoulli beam interacting with an elastic half-space. The beam representing the track-embankment system is described by Equations (2)-(4) and the parameters for the beam representing the track-embankment system are inspired from the Ledsgaard site and are given in Table 1.

Table 1: Parameters for the rail-embankment system.

		Value	Unit
<b>Rail/embankment</b>			
Cross-sectional area	$A$	10.15	$\text{m}^2$
Young's modulus	$E$	$100 \cdot 10^6$	Pa
Bending stiffness	$EI_y$	$80 \cdot 10^6$	$\text{Nm}^2$
Mass density	$\rho$	1800	$\text{kg/m}^3$
Damping coefficient	$\alpha$	0.01	[−]

The cross-sectional area are determined by considering the embankment as a 1.4 m high trapezoidal form with a width of 5.5 m in the top and a width of 9 m in the bottom. The Young's modulus and the mass density is believed to represent the material used for construction of an embankment in a reasonable way. A stiffness proportional damping is introduced in the structure with a magnitude of 1%. According to Kaynia et al. (2000) the bending stiffness is dependent on the train speed in the sense that for high train speeds the stiffness of the embankment is lower than at low train speeds. Kaynia et al. (2000) estimated the bending stiffness at the speeds of 70 and 200 km/h and the value adopted in the reference case is at a train speed of 200 km/h. The influence of the bending stiffness of the track-embankment structure is investigated in the parameter study in order to examine the importance of the parameter.

The soil is modelled as an elastic half-space. Different stratifications of the half-space is considered in the parameter study. The stratifications is a combination of the materials sand, clay and peat.

Hence, materials with significant deviation in the characteristic soil parameters are investigated. The reference parameters for these types of soils are given in Table 2.

Table 2: The soil parameters for the reference cases.

	Symbol	Value	Unit
<b>Peat</b>			
Young's modulus	$E$	$4 \cdot 10^6$	Pa
Poisson's ratio	$\nu$	0.48	[−]
Material damping	$\eta$	0.05	[−]
Mass density	$\rho$	1300	$\text{kg/m}^3$
P-wave speed	$c_P$	592	km/h
S-wave speed	$c_S$	116	km/h
R-wave speed	$c_R$	110	km/h
<b>Sand</b>			
Young's modulus	$E$	$160 \cdot 10^6$	Pa
Poisson's ratio	$\nu$	0.40	[−]
Material damping	$\eta$	0.04	[−]
Mass density	$\rho$	2000	$\text{kg/m}^3$
P-wave speed	$c_P$	1490	km/h
S-wave speed	$c_S$	608	km/h
R-wave speed	$c_R$	570	km/h
<b>Clay</b>			
Young's modulus	$E$	$15 \cdot 10^6$	Pa
Poisson's ratio	$\nu$	0.30	[−]
Material damping	$\eta$	0.045	[−]
Mass density	$\rho$	2000	$\text{kg/m}^3$
P-wave speed	$c_P$	398	km/h
S-wave speed	$c_S$	193	km/h
R-wave speed	$c_R$	177	km/h

In the parameter study four reference cases are made from these soil materials - two homogeneous half-spaces and two layered half-spaces. The homogeneous half-spaces consist of sand and clay, respectively. Thereby, the difference in behaviour of these materials are examined. However, homogeneous soil conditions are infrequent and therefore the situation of a two layered half-space is considered as well. The bottommost layers in the two layered half-spaces are the same sand and clay material as used in the homogeneous half-spaces. The top-layer in the two stratifications is a 2 m thick deposit of peat.

#### 3.1 Prestudy of the numerical model

The performance of the numerical model, which is adopted from Holm et al. (2014), is investigated in order to ensure representative results. In the prestudy simulations with a homogeneous half-space of sand and the two-layered half-space of sand and peat are considered. The constant speed  $v$  of the train in the simulations are ranging from 0.1 to 1.0 of the Rayleigh wave velocity of the sand layer. The response of the system for a variety of the simulations are illustrated in Figures 3 to 6.

Figures 3 and 4 illustrate the response along the track for the situations with the homogeneous half-

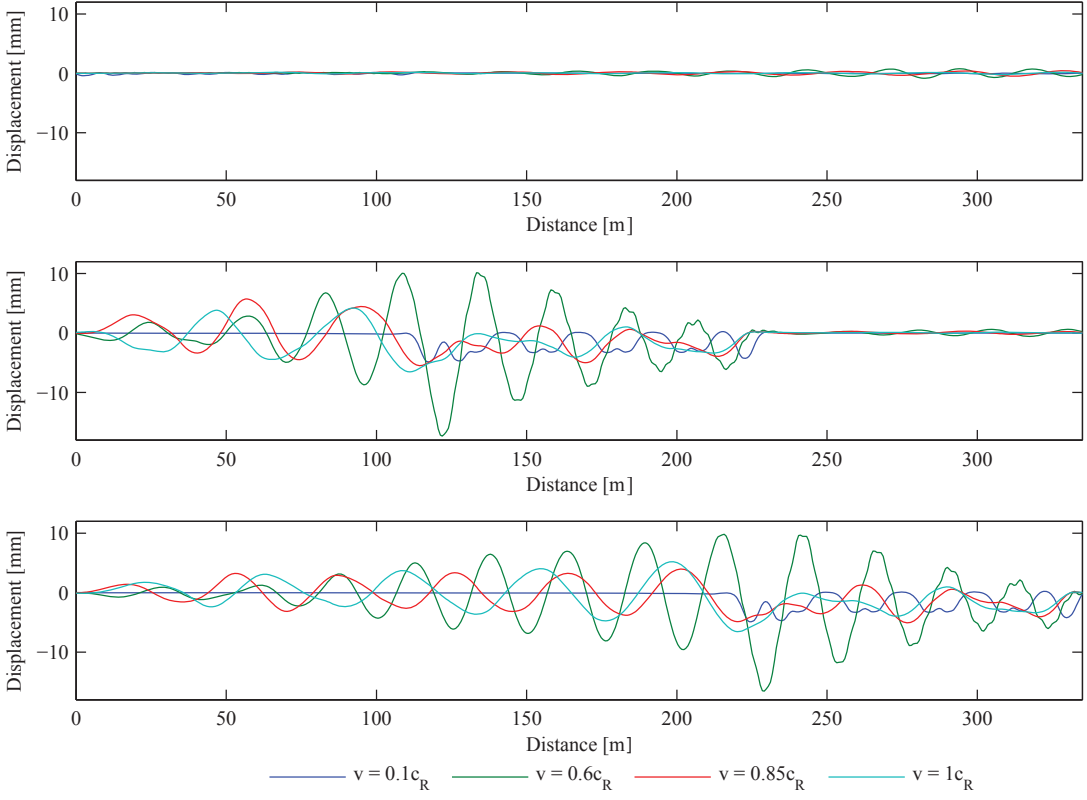


Figure 3: The vertical displacement response at different train speeds on a homogenous half-space. In (a) the front axle of the train is placed at 1/3 of the track length, in (b) 2/3 of the track length and in (c) 3/3 of the track length.

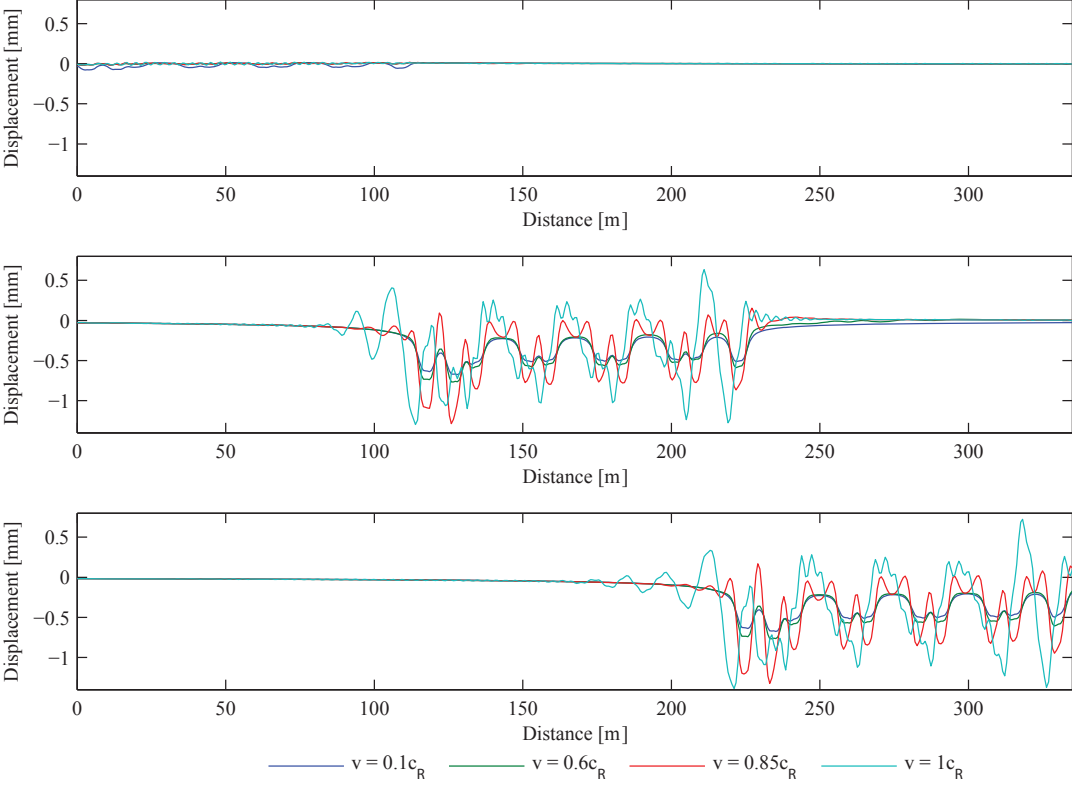


Figure 4: The vertical displacement response at different train speeds on a two-layered half-space. In (a) the front axle of the train is placed at 1/3 of the track length, in (b) 2/3 of the track length and in (c) 3/3 of the track length.

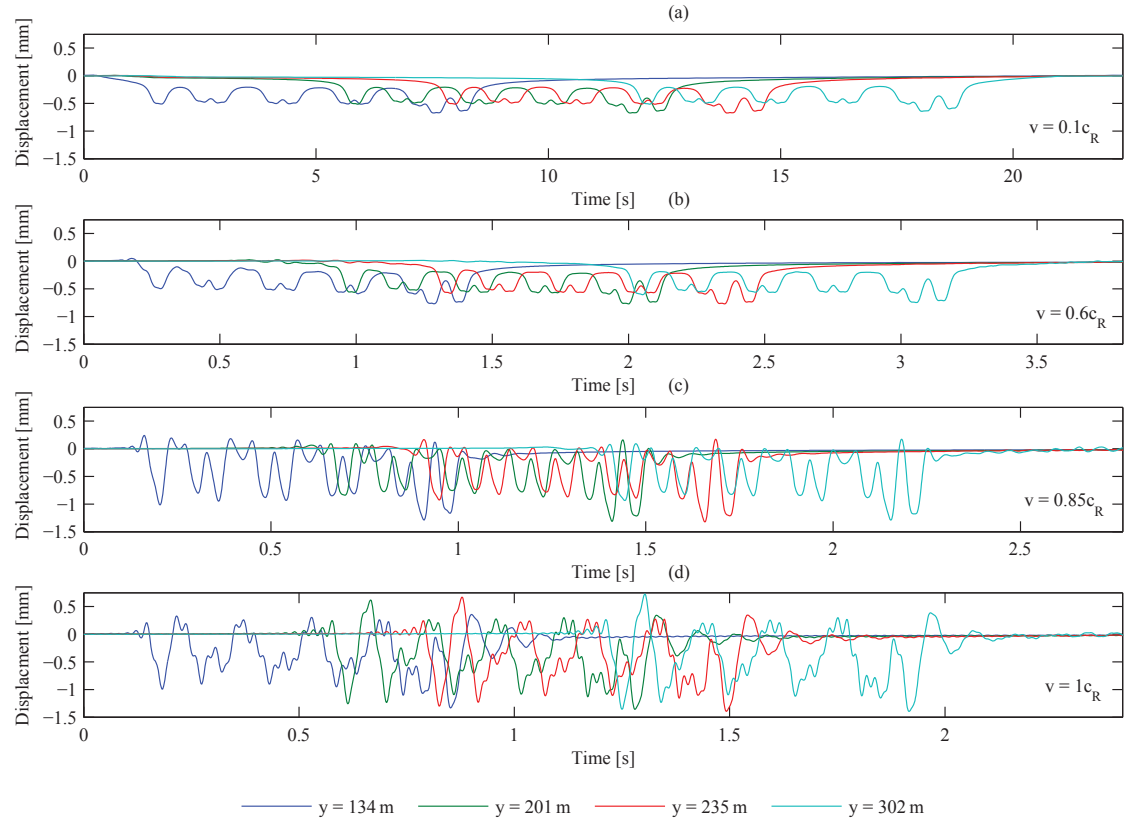


Figure 5: The vertical response for four different nodes at four relative speeds on a homogenous half-space.

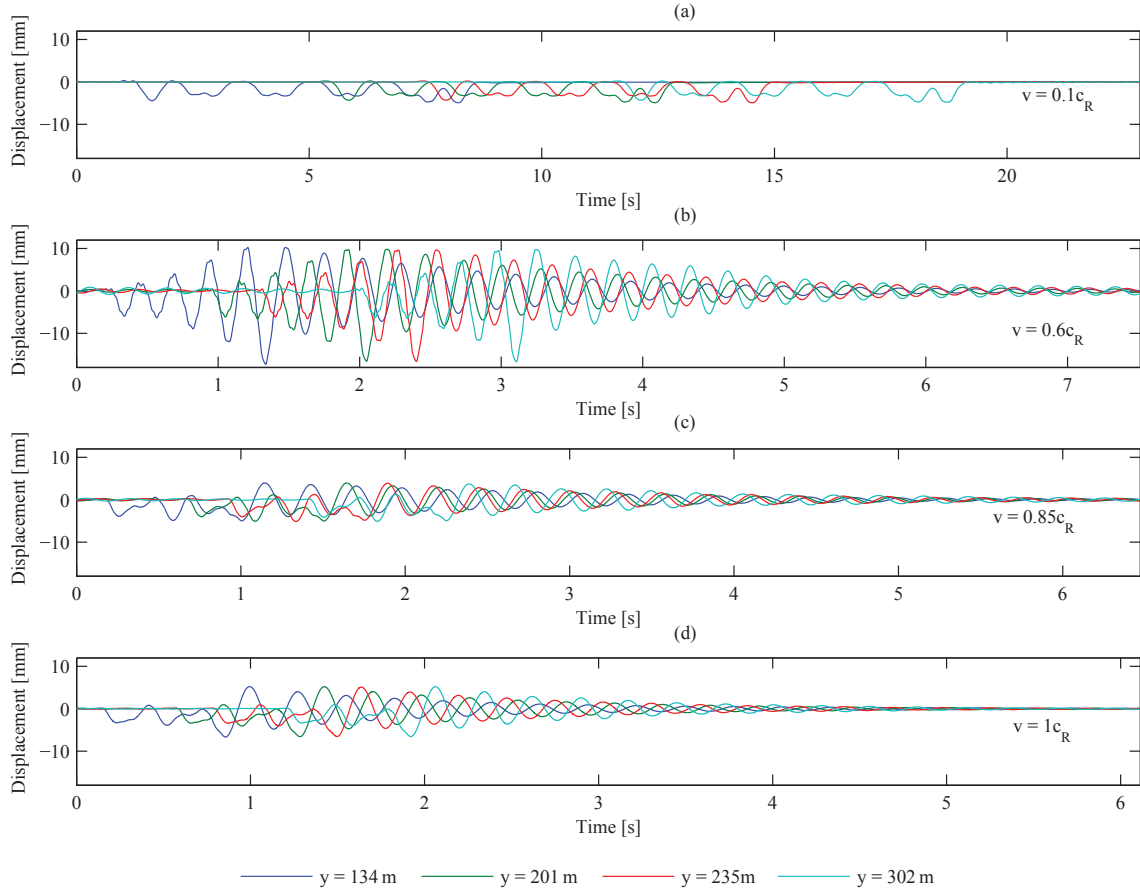


Figure 6: The vertical response for four different nodes at four relative speeds on a two-layered half-space.

space and the layered half-space, respectively. As outlined in Section 2, the railway track in the model has a total length of 335 m and the total length of the train is approximately 109 m. At the beginning of each simulation the train is located within the first 109 m of the model; thus the response of the system as the front axle of the train passes the 1/3 point in the model is only developed to a minimum. This is the situation illustrated in Figures 3a and 4a. As the train travels further through the model and the front axle passes the 2/3 point, the response becomes more pronounced. This is illustrated in Figures 3b and 4b. To confirm if the response of the system is fully developed when the front axle is located at the 2/3 point, the response of the system is calculated when the front axle of the train has travelled to the end of the model. This is illustrated in Figures 3c and 4c. The response patterns are almost identical, indicating that the responses of the system are fully developed.

From Figures 3 and 4 it can be seen that the response patterns of the system for low train speeds are almost identical for the homogeneous and the layered half-space, due to the quasi-static state. However, when the speed of the train increases the response pattern becomes remarkably different. When the train moves along the homogeneous half-space, the positions of the individual axles are relatively simple to identify as in the case of low train speeds. However, for the stratified half-space the response recalls a harmonic-like condition which only indicates the position of the front axle. In the case of the homogeneous half-space, a tail of free oscillations are following the train at the largest train speed, whereas the tail of free oscillations occurs at even lower train speeds and is much longer in the case of the layered half-space.

As an alternative to considering the response of the entire railway track, the response of nodes at different locations along the railway track is presented in Figures 5 and 6. Similarly to the observations made from Figures 3 and 4 the passage of each axle is relatively simply to identify for the low train speed, and for the homogeneous half-space also in the case of high train speeds. Comparing the nodal response in each simulation indicates that the pattern and displacement amplitude in the nodes located at a position of 201 m, 235 m and 302 m along the track are identical, with the node located at 134 m along the track having slightly lower displacement amplitudes because the response is not fully developed.

For the homogeneous half-space it is evident that the dynamic effects increase as the speed of the train tends to the Rayleigh wave speed of sand. In the case of the layered half-space the dynamic effect has a peak at the train speed of 60% of the Rayleigh wave speed of the sand. This can be explained by the presence of the peat layer which has a much lower Rayleigh wave speed.

Figures 3 to 6 shows that the presence of the 2 m of peat over the sand layer has a huge impact on the displacement amplitude. The tail of free oscillations behind the train increases in length as well as amplitude, and the increase in displacement amplitude is in general recognized.

From the observations made from Figures 3 to 6, the results compared in the subsequent parameter study (see Section 4) is based on an average value from the nodes in the range 201 m to 235 m along the track, since this indicates that the effects due to moving sources is fully developed in the model and the boundary effects of the finite track are insignificant. In the parameter study, simulations providing figures corresponding to those presented for the reference cases of a homogenous half-space of sand and a layered half-space of sand and peat are carried out. However, the results are presented in a different way.

Considering the four reference cases and in addition a homogeneous half-space of the peat material, the genesis of the figures presented in the parameter study is outlined. For each of the five different stratifications seven simulations are carried out, where the speed of the train is varying in the simulation. Otherwise, all the input parameters are the same. Train speeds in the range 0.1 to 1.0 of the Rayleigh wave speed are considered. In the case of the layered half-spaces it is the Rayleigh wave speed of the bottommost layer. The results of the simulations are illustrated in Figure 7. The two subfigures to the left consider the homogeneous half-spaces and the two subfigures at the right consider the layered half-spaces. In the subfigures (a) and (b) the absolute values of the magnitude of the upward and downward displacement are plotted. The dashed line describes the upward displacements and the full line describes the downward displacement. The amplitude is taken as the maximum peak amplitude in the node response. Examples of the node response is given in Figure 5 and 6. The upward displacements are small at low train speeds, whereas the downward displacements are significant due to the weight of the train. The subplots (c) and (d) in Figure 7 are based on the peak amplitudes, simply by adding the absolute values of the peak amplitudes, resulting in a measure of the total amplitude. This value is normalized with respect to the total amplitude at the lowest train speed. In this manner the first point will always have the value of 1.0 and the value at the other train speeds is the factor of dynamic amplification due to increasing train speed. The plots are made as function of the train speed in all the subplots, however in the bottommost subplots the train speed is normalized with respect to the Rayleigh wave speed. In the case of the layered half-spaces it is the Rayleigh wave speed of the bottommost layer.

In the case of homogeneous half-spaces, the pat-

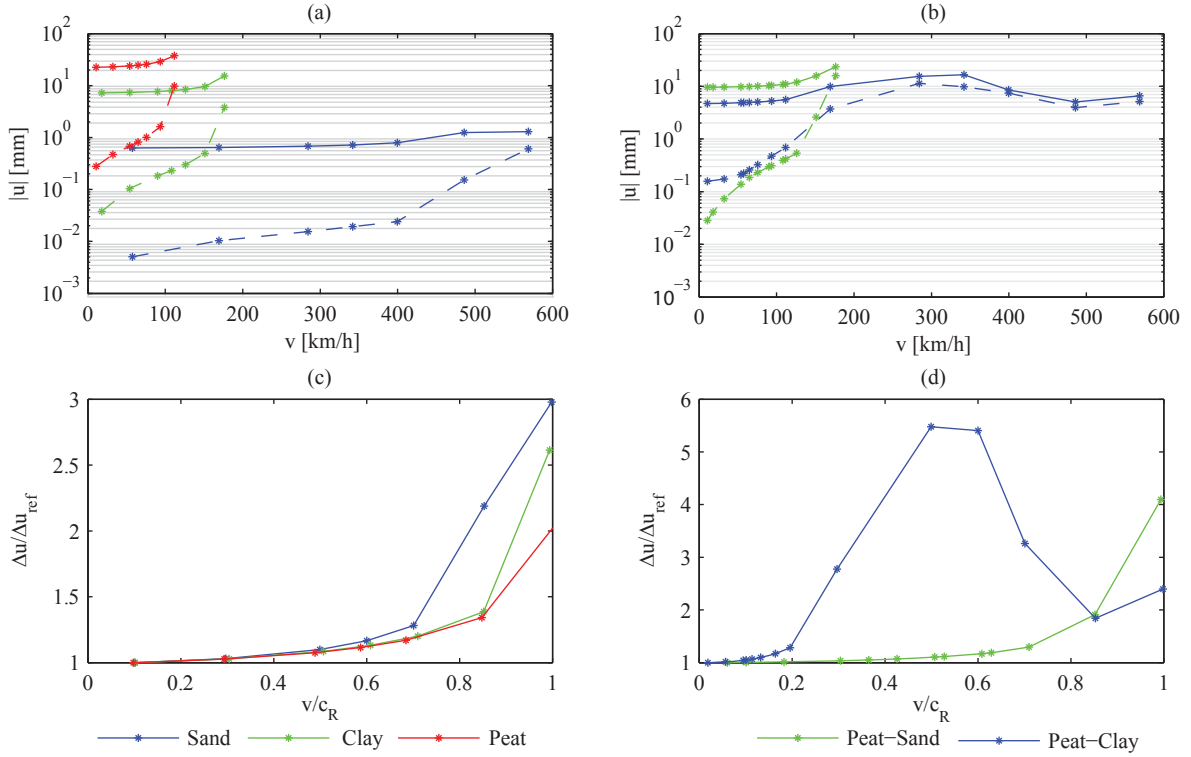


Figure 7: The dynamic amplifications due to the reference cases. Subplots (a) and (c) are related to the homogeneous half-spaces and the subplots (b) and (d) are related to the two-layered half-spaces.

tern of the graphs are quite similar; however, the values are very different due to the significantly different stiffness of the soils. In the plot of the dynamic amplification it is observed that the amplification is highest for the half-space of sand, but as seen in subplot (a), the magnitudes of the displacements are much smaller than for the clay and peat materials.

In the case of layered half-spaces the pattern is very different. This is clearly seen in subplot (d), where the situation with clay as the underlying material follows a pattern similar to the case of the homogeneous half-space of clay, with the difference being stated in the factor of dynamic amplification which is highest in the case of a layered half-space. In the case with sand, the dynamic amplification is almost doubled compared to the situation of a homogeneous half-space of sand. Furthermore, the graph shows a peak around a normalized speed of 0.5-0.6. This corresponds to the observations made from Figure 6.

Comparing the two subplots (a) and (b) it is clear, that the displacement amplitudes increase significantly when a homogeneous half-space of sand is compared to the layered half-space with sand as the underlying material. Thus, the presence of a peat layer has a significant influence. The same comparison between the two situations with clay, reveals that the influence is much less significant. The reason for this is the significant difference between

the sand and the peat material, whereas the clay and peat materials are closer related, due to the impedance mismatch discussed in Section 1.2.

From the two subplots (a) and (b) it is observed that for increasing train speeds the upward displacement amplitude tends to attain the same magnitude as the downward displacement amplitude. This is clearly observed for the layered half-space consisting of peat and sand, where the displacement amplitudes are almost alike for high train speeds, but still with the downward displacement amplitude as the largest, presumably due to the weight of the train.

## 4 Parameter study

In this section the sensitivity regarding some of the input parameters in the numerical model is studied.

### 4.1 The influence of the soil parameters

In the numerical model the soil is described by Young's modulus, Poisson's ratio, the mass density and the material damping. These parameters are used for the calculation of the characteristic wave speeds in the soil using Equation (1) with the complex Lamé constants defined as

$$\mu(\omega) = \frac{E(1 + i(\text{sign}\eta + \frac{\eta\omega}{2\pi 100}))}{2(1 + \nu)}$$

$$\lambda(\omega) = 2\mu(\omega) \frac{\nu}{1 - 2\nu}$$

implying that hysteretic damping in combination with linear viscous damping is used in the model and that the hysteretic damping and linear viscous damping are equal at 100 Hz.

In the parameter study the influence of a change in these parameters are studied. However, the influence of the mass density is not considered, since this parameter is assumed to be of minor variation and it is relatively easy obtained by simple field tests. In the case of the layered half-spaces it is the soil parameters in the top-layer of peat which are varied.

- The Young's modulus is the primary parameter dictating the wave speeds in the soil materials. An increase of Young's modulus leads to an increase of the wave speeds in the material.

- Also, Poisson's ratio has an influence on the wave speeds. An increase of Poisson's ratio will lead to an increase in the speed of the waves, especially the speed of the P-wave becomes large in comparison with the S-wave and Rayleigh wave. Poisson's ratio of soil is dependent on the material and if it is drained or undrained behaviour. If soil behaves undrained, Poisson's ratio goes towards a value of 0.5.

- The material damping occurs due to the transformation of mechanical energy into thermic energy. It describes the damping in the material and often no reliable information exist about the energy loss (Andersen, 2006). Therefore it is of interest to investigate the influence of the loss factor.

The results due to the variation of the parameters are shown in Figures 8 to 10.

In Figure 8 where a homogeneous half-space is considered in the two plots (a) and (c), it is shown in (c) that the strong increase in the dynamic amplification is between 0.7-0.9 of the Rayleigh wave

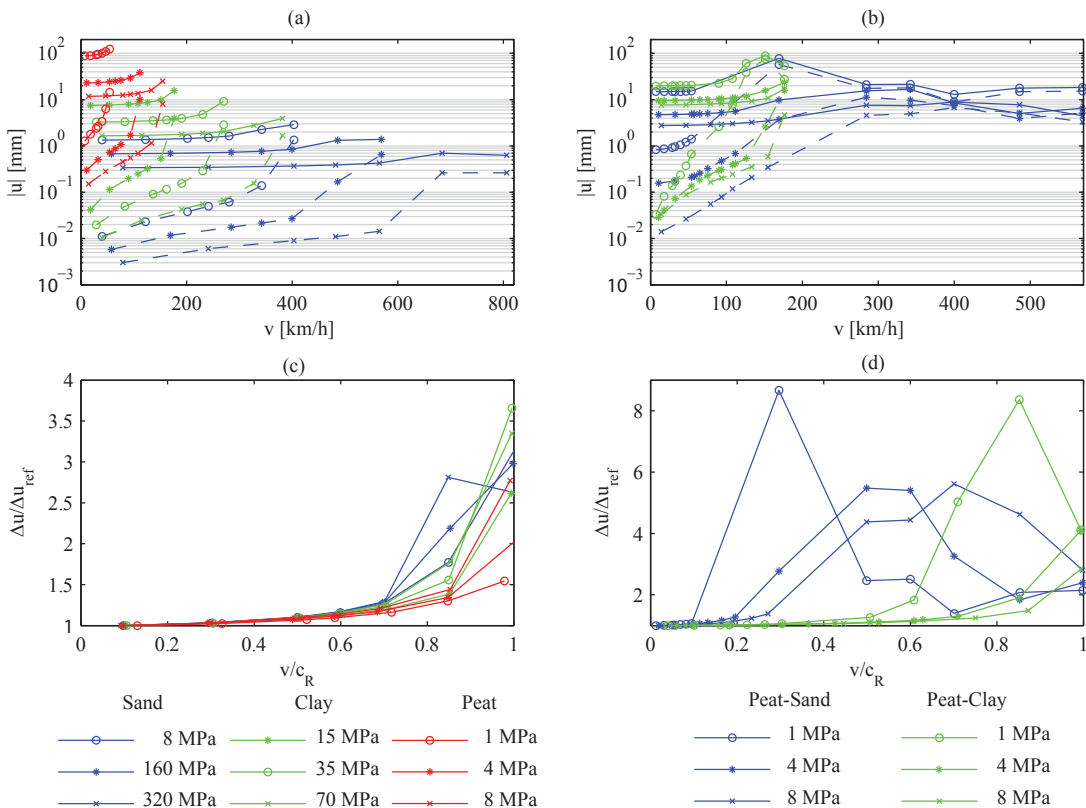


Figure 8: The Young's modulus influence on the dynamic amplification for a homogenous half-space and for a two-layered half-space of peat over sand and of peat over clay. In the upper plot the dashed symbolise the positive displacements and the solid line the absolute value of the negative displacements.

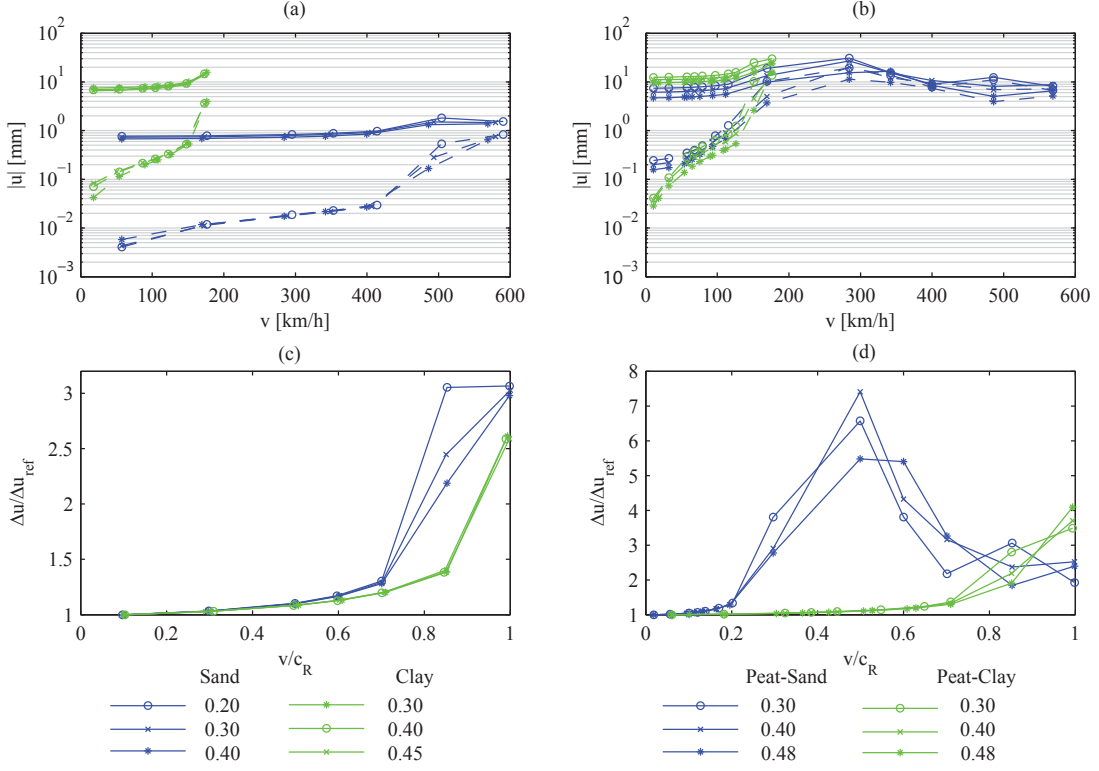


Figure 9: Influence of Poisson's ratio on the dynamic amplification for homogenous half-spaces and for two-layered half-space of peat over sand and of peat over clay. In the upper plots the dashed curves symbolize the positive displacements and the solid lines indicate the absolute value of the displacements.

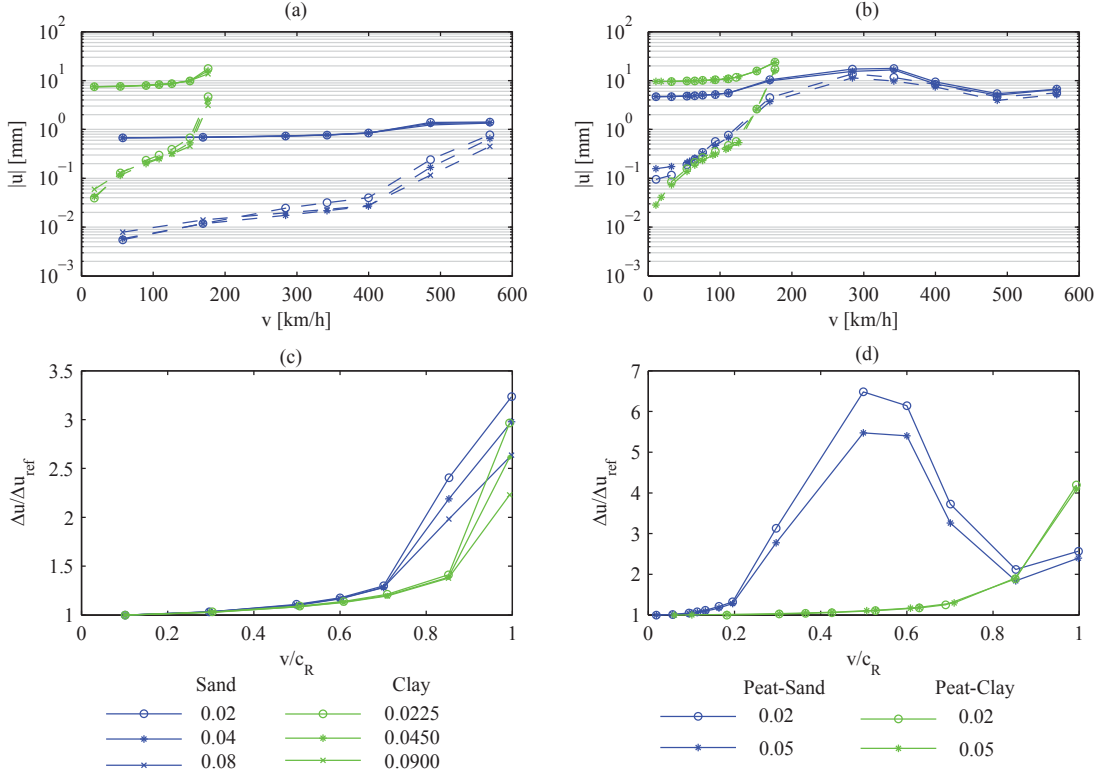


Figure 10: Influence of the loss factor on the dynamic amplification for homogenous half-spaces and for two-layered half-spaces of peat over sand and of peat over clay. In the upper plots the dashed curves symbolize the positive displacements and the solid lines indicate the absolute value of the displacements.

speed more or less independently of Young's modulus. The amplitude of the dynamic amplification is dependent on Young's modulus and the tendency is that an increase in Young's modulus gives rise to an increase in the amplitude. For the two layered half-spaces, the Figures 8(b) and 8(d) indicate that Young's modulus has a significant influence on the dynamic amplification. A low Young's modulus leads to a strong decrease in the train speed for which the dynamic amplification increases. This can be explained by the increase of the impedance ratio between the two materials. The more the two materials behave like each other, in terms of mechanical impedance the more energy will be transmitted.

On Figure 9, the dynamic amplification is shown for different values of Poisson's ratio. For Figures 9 (a) and (c) where homogenous half-spaces of sand and clay are considered, it is shown that Poisson's ratio does not have an influence on when the dynamic amplification occurs. For the two layered half-space in Figures 9 (b) and (d) Poisson's ratio for the peat is varied. The reference value is 0.48 due to the assumption of a nearly undrained behaviour. If the peat was drained, Poisson's ratio would decrease and two lower values are considered. As shown in the figures, a decrease of Poisson's ratio leads to an increase of the magnitude of the dynamic amplification, but still there is no influence on the train speed that leads to dynamic amplification.

Figures 10 (a) and (c), where homogenous half-spaces of sand and clay are considered, indicate that the loss factor does not have an influence on when the strong increase in the dynamic amplification occurs, but a low loss factor gives rise to an increasing magnitude of the dynamic amplification. In Figure 10 (a) it can be observed that the loss factor has no influence on the negative displacement, but a variation in the positive displacements is recorded. A larger loss factor gives a smaller positive displacement. For the two-layered half-space, reported in Figures 10 (a) and (c), a decrease of the loss factor from 0.05 to 0.02 (in the peat over sand and clay, respectively) indicates that the loss factor has no major influence on the dynamic amplification.

#### 4.2 The depth of the topsoil layer

In the following study the depth of the upper layer is varied. The reference depth of the peat layer is 2 m. The depth of the layer has an influence on which waves that occur in the soil and the Rayleigh wave has almost all energy in a depth two times the length of the Rayleigh wave. This means that if the upper layer has a depth larger than two times the length of the Rayleigh wave, the Rayleigh wave will not interact with the layer below. Formally the Rayleigh wave only exists in this case. In Figure 11 (b) the dynamic amplification is shown, and it can be seen that an increase of the depth of the soft

layer causes a decrease in the train speed at which the dynamic amplification occurs. The explanation of this can be that with an increase of the depth of the soft top-layer, the real surface wave speed for the soil profile will decrease and go towards the Rayleigh wave speed for the peat.

#### 4.3 Stiffness of the embankment

The bending stiffness of the track-embankment structure is a difficult size to determine accurately, since it can be discussed how much of the embankment that contributes to the bending stiffness and it can be discussed what line the embankment has rotation in. In addition, a solution of the problem of the dynamic amplification may be an improvement of the embankment. Therefore, the bending stiffness of the embankment is a central value to investigate for the impact on the dynamic amplification. As shown in Figure 12 an increase in the bending stiffness of the track-embankment structure means that the dynamic amplification is reduced and the reduction increases as the train speed goes towards the Rayleigh wave speed. The figures for the two-layered half-spaces, i.e. Figures 12 (b) and (d) indicate that an increase of the bending stiffness moves the point where the dynamic amplification increases. The magnitudes of amplification have their maxima

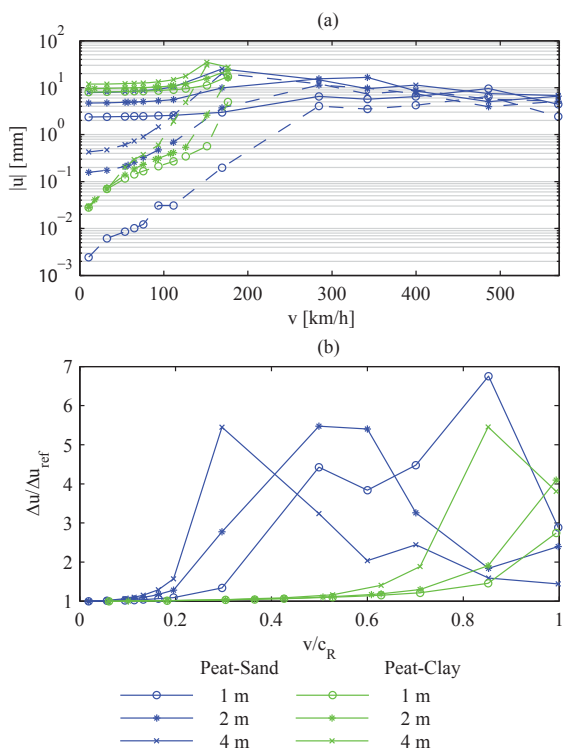


Figure 11: The depth of the soft peat layers impact on the dynamic amplification for a two layered half-space of peat over sand and of peat over clay. In the upper plot the dashed symbolise the positive displacements and the solid line the absolute value of the negative displacements.

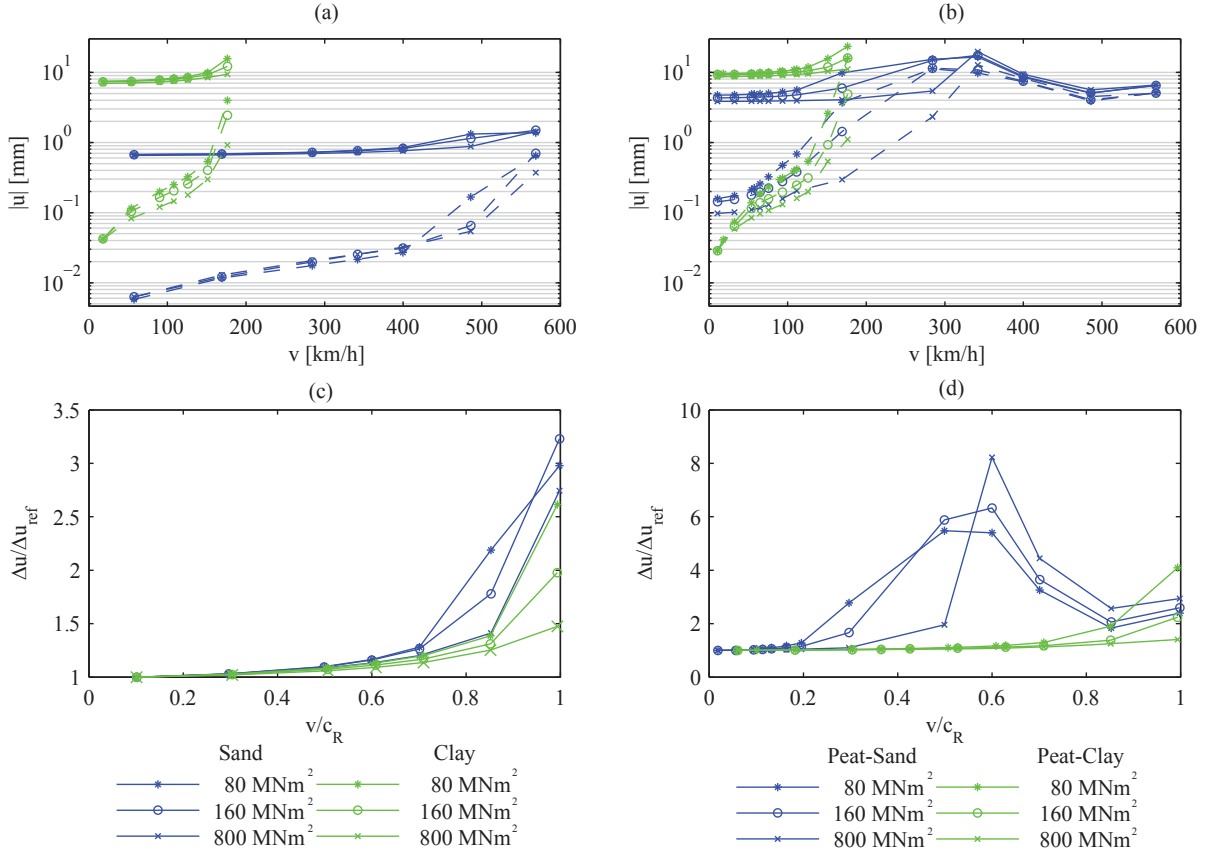


Figure 12: The bending stiffness of the embankment influences on the dynamic amplification for a homogenous half-space and for a two layered half-space of peat over sand and of peat over clay. In the upper plots the dashed symbolise the positive displacements and the solid line the absolute value of the negative displacements.

at 0.6 of the Rayleigh wave speed of the sand for the profile with peat over sand. For the profile with peat over clay, the visible maxima are at the Rayleigh wave speed of the clay.

## 5 Conclusion

On various locations the dynamic amplification of deformations in railways has shown to be a factor which can be critical. In this paper a parameter study of the dynamic amplification of deformations in railways due to high-speed trains has been presented. The study is based on a numerical model where the ground is modelled as a homogeneous or layered half-space and the track-embankment structure is modelled as a Euler-Bernoulli beam.

As a base for the parameter study some reference cases are set up including both a homogenous half-space and a two-layered half-space with a soft layer over a stiffer layer. Before the studies of the parameters, some considerations to secure reliable results from the model are done.

The parameter study indicates that the bending stiffness of the track-embankment structure does have an influence on the train speed at which dynamic amplification occurs, but it has no influence on the magnitude of the dynamic amplification. The

depth of a soft layer over a stiffer layer has an influence on when the dynamic amplification occurs as well as on the magnitude.

In the study of the influence of the soil parameters, it is observed that the Young's modulus has a significant influence regarding the train speed at which the phenomenon of dynamic amplification occurs, but if the speed is normalised with respect to the Rayleigh wave speed for the soil, it occurs at the same point. The values of Poisson's ratio and the material damping are of minor importance. From the simulations it is observed that the stratification in general has a significant impact on the response; hence focus should be on the stratification rather than the exact value of the parameters — except the stiffness in terms of Young's modulus. Especially the relative stiffness of a top-layer compared to that of an underlying half-space has been formed to be crucial regarding dynamic amplification.

## References

- Adolfsson, Andréasson, Bengtsson, and Zackrisson, 1999.** K. Adolfsson, B. Andréasson, P. Bengtsson, and P. Zackrisson. *High speed train X2000 on soft organic clay - measurements in Sweden*. Geotechnical Engineering for Transportation Infrastructure, 3, 1713–1718, 1999.
- Andersen, 2006.** L.A. Andersen. *Linear Elastodynamic Analysis*, 2006.
- Auersch, 1994.** L. Auersch. *Wave propagation in layered soils: Theoretical solution in wavenumber domain and experimental results of hammer and railway traffic excitation*. Journal of Sound and Vibration, 173, 233–264, 1994.
- Costa, Calcada, Cardoso, and Bodare, 2010.** P.A. Costa, R. Calcada, A.S. Cardoso, and A. Bodare. *Influence of soil non-linearity on the dynamic response of high-speed railway tracks*. Soil Dynamics and Earthquake Engineering, 30, 221–235, 2010.
- Holm, Riis, and Andersen, 2014.** S. Holm, A.E. Riis, and L. Andersen. *Modelling of dynamic amplification of deformations in railways due to high-speed traffic on soft ground*. 2014.
- Karlström and Boström, 2006.** A. Karlström and A. Boström. *An analytical model for train-induced ground vibrations from railways*. Journal of Sound and Vibration, 292, 221–241, 2006.
- Kaynia, Madshus, and Zackrisson, 2000.** A.M. Kaynia, C. Madshus, and P. Zackrisson. *Ground Vibration from High-Speed Trains: Prediction and Countermeasure*. Journal of Geotechnical and Geoenvironmental Engineering, 126, 531–537, 2000.
- Madshus and Kaynia, 2000.** C. Madshus and A.M. Kaynia. *High-speed railway lines on soft ground: Dynamic behaviour at critical train speed*. Journal of Sound and Vibration, 231, 689–701, 2000.
- Paolucci, Maffei, Scandella, Stupazzini, and Vanini, 2003.** R. Paolucci, A. Maffei, L. Scandella, M. Stupazzini, and M. Vanini. *Numerical prediction of low-frequency ground vibrations induced by high-speed trains at Ledsgaard, Sweden*. Soil Dynamics and Earthquake Engineering, 23, 425–433, 2003.
- Takemiya, 2003.** H. Takemiya. *Simulation of track-ground vibrations due to a high-speed train: the case of X-2000 at Ledsgaard*. Journal of Sound and Vibration, 261, 503–526, 2003.
- Woldringh and New, 1999.** R.F. Woldringh and B.M. New. *Embankment design for high speed trains on soft soils*. Geotechnical Engineering for Transportation Infrastructure, 3, 1703–1712, 1999.
- Yang and Hung, 2009.** Y.B. Yang and H.H. Hung. *Wave propagation for train-induced vibrations*. World Scientific Publishing, 2009. ISBN 978-981-283-582-6.



*Talent hits a target no one else can hit;  
Genius hits a target no one else can see.*  
— Arthur Schopenhauer